ADVANCED HEALTHCARE MATERIALS
www.advhealthmat.de

ROS Scavenging Nanozyme Modulates Immunosuppression for Sensitized Cancer Immunotherapy

Wenjing Mo, Shujie Liu, Xiaozhi Zhao, Fayun Wei, Yuhang Li, Xinan Sheng, Wenmin Cao, Meng Ding, Wenlong Zhang, Xiaoqing Chen, Longxiyu Meng, Sheng Yao, Wenli Diao, Hui Wei,* and Hongqian Guo**

Myeloid-derived suppressor cells (MDSCs) and tumor-associated macrophages (TAMs), two immunosuppressive myeloid components within the tumor microenvironment (TME), represent fundamental barriers in cancer immunotherapy, whereas current nanomedicines rarely exert dual modulatory roles on these cell types simultaneously. Reactive oxygen species (ROS) not only mediates MDSC-induced immunosuppression but also triggers differentiation and polarization of M2-TAMs. Herein, an ROS scavenging nanozyme, Zr-CeO, with enhanced superoxide dismutase- and catalase-like activities for renal tumor growth inhibition is reported. Mechanistically, intracellular ROS scavenging by Zr-CeO significantly attenuates MDSC immunosuppression via dampening the unfolded protein response, hinders M2-TAM polarization through the ERK and STAT3 pathways, but barely affects neoplastic cells and cancer-associated fibroblasts. Furthermore, Zr-CeO enhances the antitumor effect of PD-1 inhibition in murine renal and breast tumor models, accompanied with substantially decreased MDSC recruitment and reprogrammed phenotype of TAMs in the tumor mass. Upon cell isolation, reversed immunosuppressive phenotypes of MDSCs and TAMs are identified. In addition, Zr-CeO alone or combination therapy enhances T lymphocyte infiltration and IFN-γ production within the TME. Collectively, a promising strategy to impair the quantity and function of immunosuppressive myeloid cells and sensitize immunotherapy in both renal and breast cancers is provided.

1. Introduction

The emergence of immune checkpoint blockade (ICB) therapy targeting programmed death 1 (PD-1) and programmed death ligand-1 (PD-L1) has brought new prospect for responders with advanced cancers. Clear cell renal cell carcinoma (ccRCC), which constitutes almost 75% of RCC cases, is benefited by the ICB therapy because of its immunogenic nature with highly infiltrated T cells.[1] Till now, the US Food and Drug Administration has approved five ICB regimens in total for not only second-line (nivolumab, 2015) but also first-line (four combined therapies, 2018–2021) treatment of patients with metastatic renal cancers.[2] Unfortunately, as with other cancers, the efficacy of ICB monotherapies toward ccRCC is modest, with objective response rates among 20–33.6%.[3] Therefore, innovative strategies should be unearthed to improve the efficacy of current ICB therapeutics.

The immunosuppressive tumor microenvironment (TME), predominantly composed of myeloid-derived

W. Mo, Y. Li, X. Chen, H. Guo
Department of Urology
Nanjing Drum Tower Hospital Clinical College of Nanjing University of Chinese Medicine
Nanjing, Jiangsu 210008, China
E-mail: dr.ghq@nju.edu.cn

W. Mo, X. Zhao, F. Wei, Y. Li, W. Cao, M. Ding, W. Zhang, X. Chen, L. Meng, W. Diao, H. Guo
Department of Urology
Nanjing Drum Tower Hospital
the Affiliated Hospital of Nanjing University Medical School
Institute of Urology Nanjing University
321 Zhongshan Rd, Nanjing, Jiangsu 210008, China
E-mail: diaowl@126.com

The ORCID identification number(s) for the author(s) of this article can be found under https://doi.org/10.1002/adhm.202300191

DOI: 10.1002/adhm.202300191

S. Liu, H. Wei
Department of Biomedical Engineering
College of Engineering and Applied Sciences
Nanjing National Laboratory of Microstructures
Jiangsu Key Laboratory of Artificial Functional Materials
Nanjing University
Nanjing, Jiangsu 210023, China
E-mail: weihui@nju.edu.cn

X. Sheng
Key Laboratory of Carcinogenesis and Translational Research (Ministry of Education/Beijing)
Department of Genitourinary Oncology
Peking University Cancer Hospital & Institute
Beijing 100142, China

S. Yao
Shanghai Junshi Biosciences Co., Ltd.
200126Shanghai, China

S. Yao
TopAlliance Biosciences, Inc.
Rockville, MD 20850, USA

suppressor cells (MDSCs) and tumor-associated macrophages (TAMs), represents a crucial factor in immunotherapeutic resistance. MDSCs facilitate tumor progression and resistance to ICB treatments through various mechanisms, including depletion of arginine and cysteine, generation of reactive oxygen species (ROS) and nitric oxide (NO), production of cytokines, and induction of regulatory T cells (Tregs).[4] Among these mechanisms, consumption of nutrients and elevation of oxidative stress directly elicit T cell receptor (TCR) ζ chain loss, nitration or nitrosylation, and T cell proliferative arrest. Granulocytic-MDSCs (G-MDSCs) and monocytic-MDSCs (M-MDSCs), the two main subtypes of MDSCs, exploit augmentations of ROS and inducible nitric oxide synthase (iNOS), respectively, and elevation of arginase 1 both, to prompt their major immunosuppressive activities. As expected, eliminating MDSC immunosuppression via reducing ROS, arginase 1 or iNOS indeed enhanced antitumor immune response and benefited ICB treatment in RCC and other cancers.[5]

TAM phenotypes are highly plastic, which play diverse roles within the TME. In ccRCC, even the TAMs with a more pro-inflammatory phenotype in responders exhibited immunosuppressive expression changes during ICB therapy, which resulted in eventual resistance.[6] Similar to MDSCs, ROS generation is also prevalent in activated macrophages, and is necessary for the differentiation and polarization of the M2 phenotype via ERK and STAT3 activation.[7] In addition, although M2-TAM repolarization has been explored as a promising strategy to benefit ICB therapy, ignoring the hypoxic nature of tumors may result in insufficient repolarization and limit the final effect.[8] In this regard, inhibition of oxidative stress with various attempts effectively repolarized M2-TAMs and sensitized immunotherapy.[7a,9]

Nanoparticle (NP)-assisted combinatorial therapies have emerged as an attractive strategy to reshape the immunosuppressive TME, unleash antitumor responses, and thus offer enhanced ICB efficacy.[10] Recently, a few nanomodulators were designed to manipulate MDSC immunosuppression or repolarize M2-TAMs autonomously, and revealed important roles in enhancing antitumor immunity.[9b,11] However, these nanomodulators rarely exerted dual effects that alleviated the immunosuppressive roles of MDSCs and macrophages simultaneously. Given the relationship between ROS and the immunosuppressive capacity of MDSCs as well as the differentiation and polarization of M2-TAMs, we hypothesized that ROS scavenging nanomaterials might enhance the ICB response through MDSC and TAM modulation.

As the next generation of artificial enzymes, nanozymes have been extensively exploited owing to their superior properties over natural enzymes and conventional enzyme mimics, such as multienzyme-like activities and multifunctionalities.[12] In particular, various nanozymes have been developed to scavenge ROS by mimicking the activities of catalase (CAT), superoxide dismutase (SOD), glutathione peroxidase, etc.[12m,13] Among them ceria nanozyme has been widely used to regulate oxidative stress for biomedical applications because of its excellent CAT- and SOD-like activities.[14] Since the ratio of Ce^{3+}/Ce^{4+} plays a key role in ROS scavenging, it is feasible to enhance the antioxidant activity of ceria by modulating the Ce^{3+}/Ce^{4+} ratio.[12h,15] Zuo et al. designed a nanoplatform in which ceria converted endogenous H_2O_2 to O_2 at tumor sites, and reduced the population and function of tumor-infiltrated MDSCs in melanoma.[16] To date, in regard to malignant tumors, few studies on the role of ceria nanozyme in MDSCs and TAMs have been performed.

In this study, we developed Zr-CeO nanozyme with an enhanced ratio of Ce^{3+}/Ce^{4+} via Zr^{4+} doping.[12h] Zr-CeO enabled dual intracellular ROS scavenging of MDSCs and macrophages, which attenuated MDSC-induced immunosuppression and shifted M2-TAM polarization. Furthermore, Zr-CeO showed surprising effects on sensitizing ICB therapy in murine renal and breast tumor models, associated with MDSC and TAM modulation in both quantity and capacity. To the best of our knowledge, this is the first time to employ a ceria-derived nanozyme for ICB therapy improvement. As such, this simple nanoparticle remodeled the TME in two ways. First, Zr-CeO inhibited ROS-induced TCR ζ chain loss, diminished unfolded protein response (UPR) in MDSCs, and thus impaired levels of arginase 1 and iNOS; second, Zr-CeO reprogrammed ROS-dependent M2-TAM polarization through suppressing ERK and STAT3 pathways (**Scheme 1**). Thus, we provided an efficient nanomodulator that reshaped the TME and enhanced ICB therapy.

2. Results and Discussion

2.1. Synthesis and Characterization of Zr-CeO NPs

The ceria (CeO) NPs and Zr-doped ceria (Zr-CeO) NPs were synthesized through a facile wet chemical method.[17] The products were modified by citrate to endow them with boosted biocompatibility. The obtained CeO NPs were clear dark yellow, while Zr-CeO NPs were reddish brown (inset of **Figure 1**A). As shown in Figure S1A in the Supporting Information, the presence of carboxyl groups was at around 1400 and 1600 cm^{-1}, as well as hydroxyl groups at around 3400 cm^{-1} in the Fourier-transform infrared (FT-IR) spectrum, confirming the successful modification of citric acid on the surface of Zr-CeO NPs.[18] Moreover, due to the citrate on the surface, the zeta potentials of CeO and Zr-CeO NPs were −29.1 and −26.4 mV, respectively, explaining their excellent dispersions (Figure S1B, Supporting Information). And as the transmission electron microscope (TEM) images shown in Figure 1A, the spherical Zr-CeO NPs were uniform, and the average size was 3.1 nm, which was smaller than that of the pristine CeO NPs (5.6 nm) (Figure S1C, Supporting Information). The dynamic light scattering (DLS) results in Figure 1B also exhibited a consistent phenomenon, which was caused by the solute drag effect.[19] In addition, as shown in Figure 1C, the X-ray diffraction (XRD) patterns of Zr-CeO NPs were shifted to high-angle compared to CeO NPs, which can be attributed to the smaller atomic radius of Zr. The absence of any characterization peaks associated with zirconium oxide indicated the formation of a solid solution and the successful doping of Zr species. Meanwhile, the X-ray photoelectron spectroscopy (XPS) spectrum of Ce 3d of Zr-CeO NPs showed that the dopant Zr species could effectively regulate the ratio of Ce^{3+}/Ce^{4+} compared to CeO NPs, which was crucial in the SOD-like activity (Figure 1D). Of note, the ratio of Ce^{3+}/Ce^{4+} increased to 55% from 32%. Correspondingly, the Zr-CeO NPs were proven to possess better SOD-like and CAT-like activities,

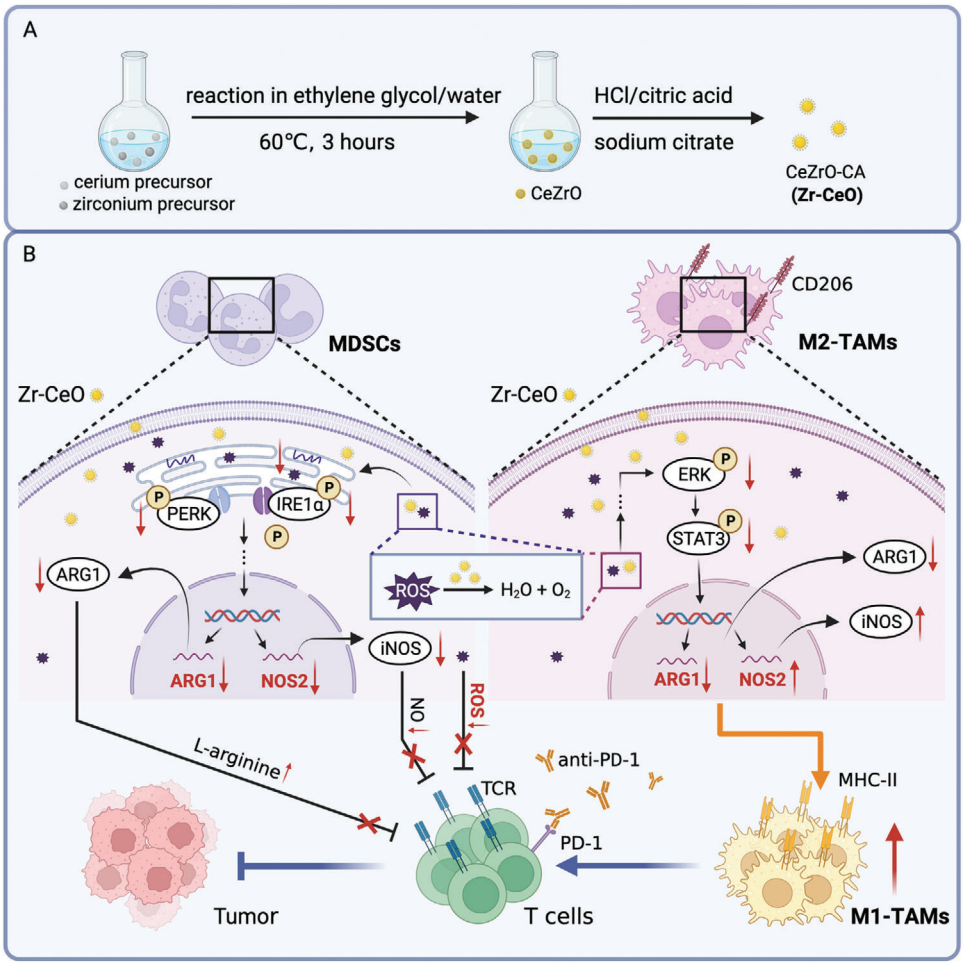

Scheme 1. A) Synthesis of Zr-CeO NPs. B) Zr-CeO nanozyme modulates the immunosuppressive function of MDSCs and the phenotype of TAMs via distinct pathways. Created with BioRender.com.

owing to the doping of Zr species (Figure 1E,F). The enhanced ROS scavenging capacity could be beneficial for immune modulation.

2.2. Zr-CeO Nanozyme Remarkably Impeded the Progression of RCC

A murine subcutaneous allograft tumor model was utilized to examine the role of Zr-CeO nanozyme in renal carcinoma. As shown in **Figure 2**A,B, Renca tumor growth was promptly restricted at the first administration of Zr-CeO and continued to be restrained until sacrifice (58.99% growth inhibition; Zr-CeO vs control: $p = 0.0004$), whereas mice body weight barely changed during this process (Figure S2, Supporting Information). The tumor weight of mice treated with Zr-CeO was less than half of that of the control group (≈0.49 g vs ≈1.20 g, Figure 2C), and nanozyme treatment effectively prolonged the survival of the tumor-bearing mice (42.5 days vs 27 days, Figure 2D). Additionally, we performed hematoxylin and eosin (H&E) staining, terminal deoxynucleotidyl transferase dUTP nickel end labeling (TUNEL), and immunohistochemistry staining to measure the growth status of the tumors. It showed that Zr-CeO treatment markedly enhanced the apoptosis and necrosis of tumor cells (Figure 2E). The treatment also reduced the ratio of Ki-67$^+$ cells from 77.30% to 54.15% (Figure 2F), which represents the proliferation level of tumors.

To study the dynamic distribution of Zr-CeO nanozyme, we subcutaneously implanted Renca tumors and injected mice with Zr-CeO when the tumors were around 140 mm^3. The harvested major tissues and tumors at various time points were subjected to inductively coupled plasma-mass spectrometry (ICP-MS) to determine the distribution of Zr-CeO nanozyme. Following a single injection, Zr element representing for Zr-CeO rapidly distributed among major organs (especially spleens and livers) and tumors, and persisted until 48 h. From 3 to 24 h after injection, the hearts, lungs, and spleens showed significant elimination of Zr, whereas the tumors showed accumulation of the nanozyme (Figure 2G). We speculated that the large amounts of ROS produced in tumors probably recruited and detained Zr-CeO and drove this dynamic distribution.[20]

The short-term (24 h) and long-term (30 days, once every 3 days) biosafety of Zr-CeO was further verified by H&E staining of the major organs. The results in Figure S3A,B in the Supporting

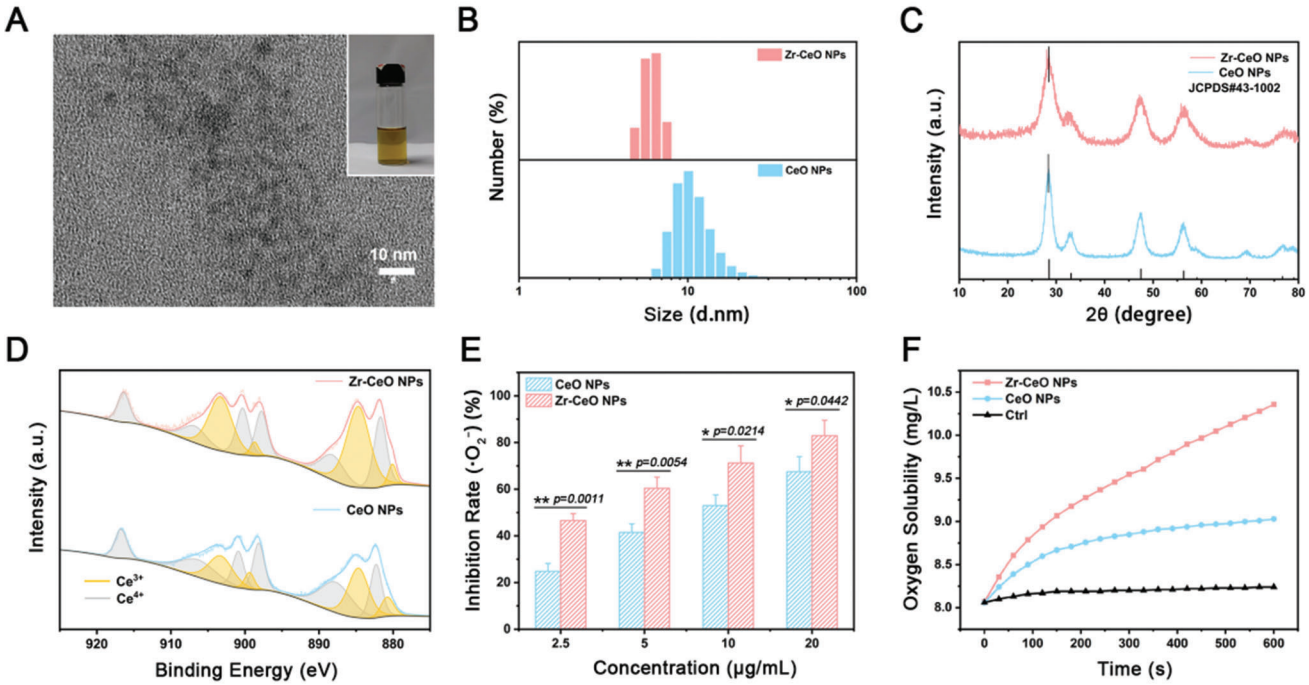

Figure 1. Structural characterizations and enzymatic ROS-scavenging activities of Zr-CeO NPs. A) TEM images of Zr-CeO NPs and digital photographs of Zr-CeO NPs solutions (insets). Scale bar: 10 nm. B) Hydrodynamic size distributions, C) XRD patterns, and D) XPS spectra of Zr-CeO NPs and CeO NPs. E) Superoxide anion inhibition rate of Zr-CeO NPs at different concentrations and F) the amount of oxygen generated by catalytically decomposing H_2O_2 with Zr-CeO NPs and CeO NPs. Data are presented as mean ± SD, $n = 3$, two-tailed Student's *t*-test. $^*p < 0.05$, $^{**}p < 0.01$.

Information showed that compared to saline group, no obvious pathological abnormalities were observed in the hearts, livers, spleens, lungs, and kidneys at the above time points. In addition, the kidney function indexes (creatinine; blood urea nitrogen, BUN) and liver function indexes (alanine aminotransferase, ALT; aspartate transaminase, AST; alkaline phosphatase, ALP) of mice remained unchanged (Figure S4, Supporting Information). These data suggest that the Zr-CeO nanozyme exhibits marked antitumor effects against renal carcinoma with favorable in vivo biosafety.

2.3. Zr-CeO Nanozyme Hardly Changed the Viability and Apoptosis of Renal Cancer Cells

Contingent upon concentration, ROS exert either pro-tumorigenic or cytotoxic effects on cancer evolution. Recently, therapeutic strategies concerning ROS generation have shown antitumor effects in RCC and breast cancer.[21] Nevertheless, cancer cells can tolerate high ROS-triggered senescence, apoptosis, and ferroptosis by modulating glutathione, thioredoxins, and NADPH generation, as well as activating antioxidant transcription factor networks.[22]

To determine whether Zr-CeO nanozyme directly affected the intracellular ROS generation in renal cancer cells, we treated Renca, 769P (human clear renal adenocarcinoma cells), and ACHN (human renal cell adenocarcinoma cells) with different concentrations of Zr-CeO. By utilizing an ROS assay kit, the data in Figure S5 in the Supporting Information suggest that Zr-CeO did not change the ROS levels in Renca and ACHN until 48 h, while it slightly reduced the ROS levels in 769P. However, even in 769P cells, the removal of ROS hardly improved the viability or suppressed the apoptosis, consistent with Renca and ACHN cells, as well as normal renal tubular epithelial cells (HK-2) (Figure S6A,B, Supporting Information). These data suggest that the Zr-CeO nanozyme had no direct effects on the growth status of renal cancer cells and no obvious cytotoxicity on normal tubular epithelial cells. Considering the nanozyme-induced apoptosis and necrosis of tumor cells in vivo, indirect pathways should be screened to clarify the underlying mechanism of the antitumor effect of Zr-CeO.

2.4. ROS Scavenging Attenuated MDSC Immunosuppression via Downregulating UPR In Vitro

Besides generation, ROS elimination has also been considered as a prospective approach to provoke antitumor immune response.[9a,23] As a vital component of TEM, the response of MDSCs to Zr-CeO nanozyme was investigated subsequently. Following the classic protocol, we induced mouse bone marrow-derived MDSCs (BM-MDSCs) with interleukin-6 (IL-6) and granulocyte-macrophage colony stimulating factor (GM-CSF) for 4 days and treated these BM cells with Zr-CeO or saline 2 days before collection. Zr-CeO treatment diminished ≈40% of intracellular ROS at a concentration of only 2.5 μg mL^{-1}, and scavenged more than half of ROS at 10 μg mL^{-1} (**Figure 3**A). ROS in MDSCs consist of hydrogen peroxide (H_2O_2) and superoxide ($O_2\bullet^-$).[24] Through SOD-like activity, Zr-CeO converted $O_2\bullet^-$ to H_2O_2, and H_2O_2 was conversed to O_2 by the CAT-like activity.[25]

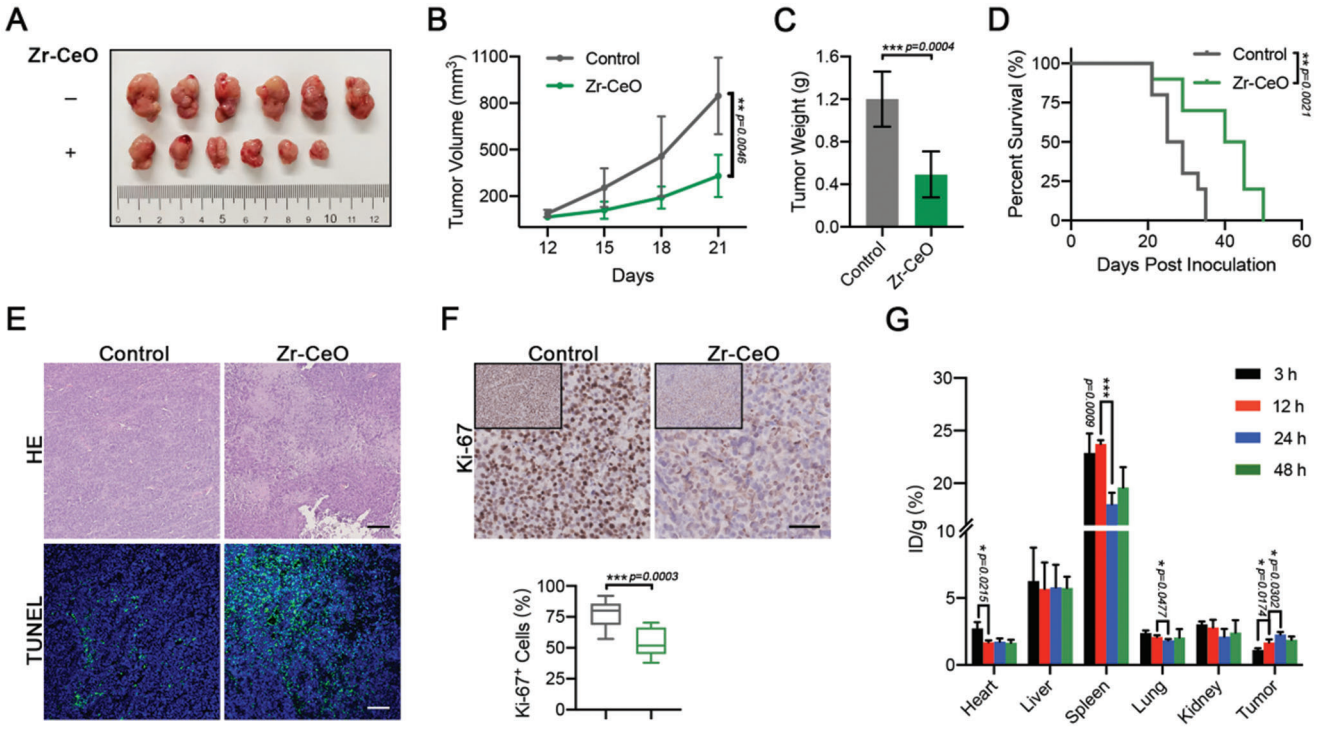

Figure 2. Antitumor effect of Zr-CeO nanozyme in renal subcutaneous tumors. A) Photograph of dissected Renca subcutaneous tumors after the fourth i.v. administration of saline or 10 mg kg^{-1} Zr-CeO (once every 3 days, $n = 6$). B) Sizes of tumors since first administration. C) Endpoint tumor weight in grams. D) Survival percentages of mice receiving different treatments ($n = 10$). E) Representative H&E and TUNEL staining of endpoint tumor sections. Scale bars: 100 μm. F) Representative immunohistochemistry staining for Ki-67 in endpoint tumor sections. Lower, quantification of the percentages of positive cells from eight high-power fields per group ($n = 6$). Scale bar: 50 μm. G) Percentages of injected dose per gram of Zr in main organs and tumors at different time points after i.v. administration of 10 mg kg^{-1} Zr-CeO ($n = 3$). Data in (B), (C), and (G) are shown as mean ± SD. Data in (F) are shown as min to max. Statistical significance in (B) was evaluated using one-way ANOVA with Tukey's test. Statistical significance in (D) was evaluated using log-rank test. Statistical significance in (C), (F), and (G) was evaluated using two-tailed Student's *t*-test. $^*p < 0.05$, $^{**}p < 0.01$, $^{***}p < 0.001$.

Moreover, the proportion of $CD11b^+Gr\text{-}1^+$ MDSCs was decreased by 10 μg mL^{-1}, especially 20 μg mL^{-1} nanozyme treatment (Figure S7A, Supporting Information), and the viability of MDSCs was inhibited in a concentration-dependent manner (Figure S7B, Supporting Information).

In addition to expansion and viability, the immunosuppressive capacity per MDSC should be taken into account under these circumstances. To evaluate the role of Zr-CeO treatment on MDSC-mediated $CD8^+$ T cell proliferative arrest, we sorted mouse splenic $CD8^+$ T cells, enforced proliferation with anti-CD3 and anti-CD28, and designed three sets of T cell proliferation assays (i: T cells alone, ii: T cells co-cultured with MDSCs pretreated with nanozyme or saline; iii: T cells co-cultured with MDSCs in the treatment of nanozyme or saline). Flow cytometry analysis showed that Zr-CeO had no significant effect on T cell proliferation directly (Figure 3B-i), whereas MDSCs pretreated with Zr-CeO for 48 h had a weakened suppressive capacity on T cell proliferation (Figure 3B-ii), indicating that Zr-CeO could restore T cell proliferation by attenuating MDSCs ability beforehand. Moreover, co-culture of T cells and MDSCs during the treatment of nanozyme showed recovered T cell proliferation (Figure 3B-iii), either, with a proliferation rate similar to the data in Figure 3B-ii, which confirmed the role that Zr-CeO played on MDSCs to reverse T cell suppression.

It has been well established that MDSCs also trigger T cell proliferative arrest or anergy through enrichment of arginase 1 and iNOS, which consume nutrients and generate NO, respectively.[5] Of note, Zr-CeO substantially downregulated both the protein (Figure 3C and Figures S8 and S32, Supporting Information) and mRNA levels (Figure S9, Supporting Information) of arginase 1 and iNOS, as well as the intracellular NO generation (Figure S10, Supporting Information). Recently, endogenous ROS-amplified endoplasmic reticulum (ER) stress and UPR have been demonstrated to enhance MDSC immunosuppression via augmenting the transcription of arginase 1 and iNOS.[26] To determine whether ROS scavenging by Zr-CeO dampened UPR and thus attenuated MDSC immunosuppression, we assessed the fluorescence of ER-tracker in MDSCs by flow cytometry. As shown in Figure 3D and Figure S11 in the Supporting Information, Zr-CeO diminished the fluorescence of ER-tracker in a dose-dependent manner, consistent with the downregulated total and phosphorylated levels of PERK and IRE1, the major modulators of UPR (Figure 3E and Figures S12 and S33, Supporting Information). Apart from the impact on UPR, Zr-CeO-induced $O_2{\bullet}^-$ depletion could probably inhibit the conversion of NO to the strong oxidant peroxynitrite ($ONOO^-$), which facilitates nitration or nitrosylation of TCR, CD8, CD3, and CCL2, impairing T cell activation and traffic.[27] However, the production of *Tgfb1* and *Il10*, representing the capacity of MDSCs to induce Tregs, was not

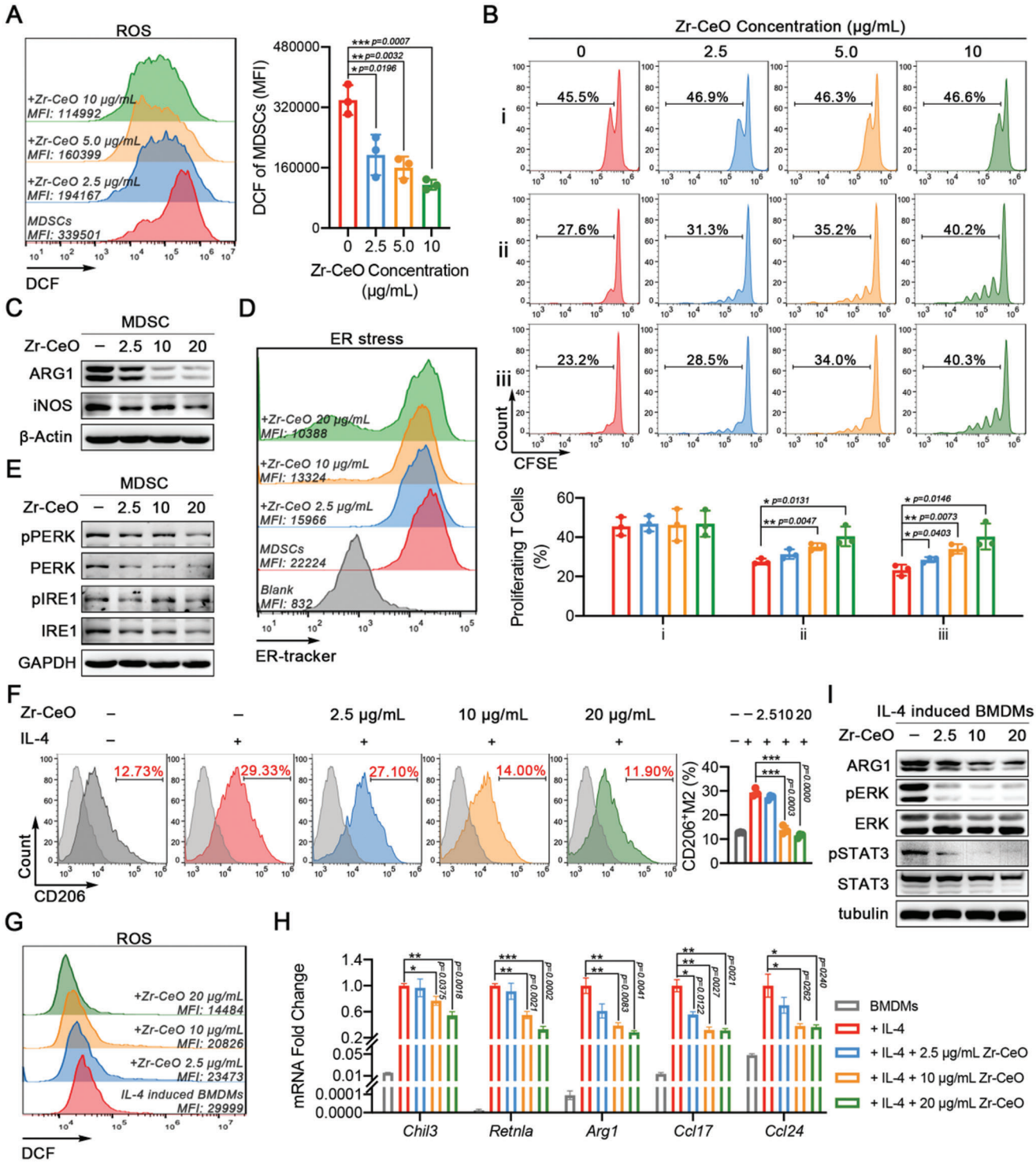

Figure 3. ROS scavenging attenuated MDSC immunosuppression and shifted M2-TAM polarization in vitro. A) Flow cytometric analysis of ROS levels in BM-MDSCs treated with different concentrations of Zr-CeO for 48 h. Right, quantification of the mean fluorescence intensity (MFI). B) Flow cytometric assessments of CFSE-labeled $CD8^+$ T cell proliferation primed with anti-CD3 and anti-CD28 under different co-culture conditions for 72 h. i) $CD8^+$ T cells treated with Zr-CeO; ii) $CD8^+$ T cells co-cultured with MDSCs that were pretreated with Zr-CeO for 48 h; iii) $CD8^+$ T cells co-cultured with MDSCs and Zr-CeO simultaneously (MDSCs vs $CD8^+$ T cells, 1:4). Lower, quantification of the percentages of proliferating T cells from three independent repeats. C) Western blot analysis of arginase 1 (ARG1), iNOS, and β-actin levels in BM-MDSCs treated with different concentrations of Zr-CeO for 48 h. D) Flow cytometric analysis of ER-tracker staining and E) western blot analysis of pPERK, PERK, pIRE1, IRE1, and GAPDH levels in BM-MDSCs treated with Zr-CeO for 48 h. F) Analysis of $CD206^+$ macrophages in 20 ng mL^{-1} IL-4-induced BMDMs treated with Zr-CeO or saline for 24 h, merged with isotype control (light gray). Right, quantification of the percentages of $CD206^+$ macrophages. G) Flow cytometric analysis of ROS levels in IL-4-induced

distinctly changed by nanozyme at the transcriptional level (Figure S9, Supporting Information). Together, these data suggest that the elimination of intracellular ROS by Zr-CeO nanozyme significantly manipulated MDSC immunosuppression in two ways. On the one hand, Zr-CeO suppressed the expansion and viability of MDSCs; on the other hand, it dampened UPR in MDSCs, thus downregulating the transcriptional levels of arginase 1 and iNOS, and attenuating the immunosuppressive capacity of MDSCs.

2.5. ROS Scavenging Shifted M2-TAM Polarization via ERK and STAT3 Pathways

Compared to MDSCs, TAMs, the other key population in the TME, exert more diverse and specific phenotypes, among which M2 subtypes repress antitumor immunity and induce angiogenesis and cancer cell migration.[28] ROS is essential in M2-TAM differentiation and polarization.[7a,29] In TAMs, the types of ROS include H_2O_2, $O_2\bullet^-$ and hydroxyl radicals ($OH\bullet$).[7a,30] Zr-CeO nanozyme with strong activities of SOD- and CAT-like activities was expected to deplete most types of ROS in TAMs. Accordingly, we investigated whether ROS scavenging by Zr-CeO nanozyme affected the polarization of M2 macrophages and TAMs. To induce bone marrow-derived macrophages (BMDMs), bone marrow cells were treated with macrophage colony stimulating factor (M-CSF) for 7 days. Then, the adherent macrophages were stimulated with IL-4 for 24 h to induce the polarization toward M2. Following IL-4 stimulation, the proportion of $CD206^+$ M2 macrophages was remarkably enhanced, whereas the introduction of Zr-CeO significantly reversed such increase (Figure 3F), accompanied with the expected decrease in the ROS level in these IL-4-induced BMDMs (Figure 3G and Figure S13, Supporting Information). Meanwhile, the expression of M2 macrophage-specific markers, including *Chil3* (YM1) and *Retnla* (Fizz1), functional gene *Arg1*, as well as chemokines *Ccl17* and *Ccl24* were also constrained by Zr-CeO treatment (Figure 3H). As stated earlier, ERK and STAT3 are pivotal signaling pathways involved in ROS-dependent M2 macrophage polarization.[7] Therefore, we examined the effect of Zr-CeO on modulating these pathways and found that ROS scavenging substantially blocked the activation of ERK and STAT3 by low concentrations of nanoparticles (Figure 3I and Figures S14 and S34, Supporting Information). Moreover, to evaluate the effect of Zr-CeO on TAM polarization in vitro, we treated human monocytic cell line THP-1 with phorbol 12-myristate 13-acetate (PMA) to obtain M0 macrophages, and co-cultured these PMA-induced M0 macrophages with the renal cancer cell line ACHN. It was found that co-culture with ACHN significantly increased the ratio of $CD206^+$ TAMs, whereas as low as 2.5 μg mL^{-1} nanozyme could diminish intracellular ROS and shift M2-TAM polarization (Figure S15A,B, Supporting Information). Collectively, these data demonstrate that intracellular ROS scavenging by Zr-CeO nanozyme inhibits $CD206^+$ M2 or TAM polarization, probably via suppressing ERK and STAT3 phosphorylation.

2.6. Zr-CeO Nanozyme Slightly Changed the Phenotype of CAFs but Barely Affected the Production of Functional Soluble Factors

Cancer-associated fibroblasts (CAFs) are another abundant component of tumor stroma, which play a crucial role in tumor progression and invasion via remodeling the extracellular matrix and secreting growth factors, cytokines, and chemokines.[31] Thus, we also investigated the effect of Zr-CeO nanozyme on CAFs. Human fibroblasts were isolated from fresh RCC tissues and their paired normal renal tissues. They were identified by immunofluorescence as normal fibroblasts (NFs), with the phenotype of α-SMA^- $vimentin^+$ $E\text{-}cadherin^-$, and as CAFs, with the phenotype of α-SMA^+ $vimentin^+$ $E\text{-}cadherin^-$, respectively (Figure S16A, Supporting Information). Treatments with three concentrations of Zr-CeO did not affect the phenotype of NFs but slightly weakened the fluorescence signals of α-SMA (alpha-smooth muscle actin) and vimentin in CAFs (Figure S16A, Supporting Information). The effect of nanozyme on downregulating α-SMA was consistent with the previous evidence that antioxidants or nanoceria at nontoxic concentrations inhibited CAFs formation and ROS-dependent expression of α-SMA.[32] However, Zr-CeO treatment (both 24 and 48 h) barely impaired the viability of CAFs (Figure S16B,C, Supporting Information). The mRNA levels of the CAF specific marker, *FAP*, and CAF specific cytokines, chemokines, and growth factors, including *IL6*, *TGFB1*, *CCL2*, *CXCL1*, *CXCL8*, *CXCL12*, *CXCL16*, *HGF*, *VEGFA*, *LIF*, and *IGF1*, showed no significant changes after treatment with 10 μg mL^{-1} Zr-CeO for 24 h (Figure S16D,E, Supporting Information). These data indicate that Zr-CeO nanozyme slightly changed the phenotype of renal CAFs but barely affected their viability and production of functional soluble factors.

2.7. Zr-CeO Nanozyme Enhanced the Antitumor Efficacy of PD-1 Inhibition in a Mouse Model of RCC

Given the dual effects of Zr-CeO on attenuating MDSC immunosuppression and shifting M2-TAM polarization in vitro, we evaluated whether Zr-CeO could enhance the efficacy of anti-PD-1 immunotherapy in vivo. Renca subcutaneous tumor-bearing mice were randomly divided into four groups with periodic treatment of saline, anti-PD-1 (10 mg kg^{-1}), Zr-CeO (10 mg kg^{-1}) or the combination of anti-PD-1 and Zr-CeO (**Figure 4**A). Treatment with nanozyme alone led to remarkable inhibition of tumor growth (66.00% growth inhibition; Zr-CeO vs control: $p = 0.0001$), while anti-PD-1 alone only moderately suppressed tumor growth (37.43% growth inhibition; anti-PD-1 vs control: $p = 0.0190$) (Figure 4B–D). The combination therapy was most effective in inhibiting tumor growth compared with any other group (82.47% growth inhibition; combination

BMDMs treated with Zr-CeO for 24 h. H) RT-qPCR analysis of the levels of M2 macrophage-specific markers (*Chil3*, *Retnla*), functional gene (*Arg1*), and chemokines (*Ccl17*, *Ccl24*) in IL-4-induced BMDMs with Zr-CeO treatments. I) Western blot analysis of ARG1, pERK, ERK, pSTAT3, STAT3, and tubulin in IL-4-induced BMDMs with Zr-CeO treatments. Data are presented as mean ± SD, $n = 3$, two-tailed Student's *t*-test. $^*p < 0.05$, $^{**}p < 0.01$, $^{***}p < 0.001$.

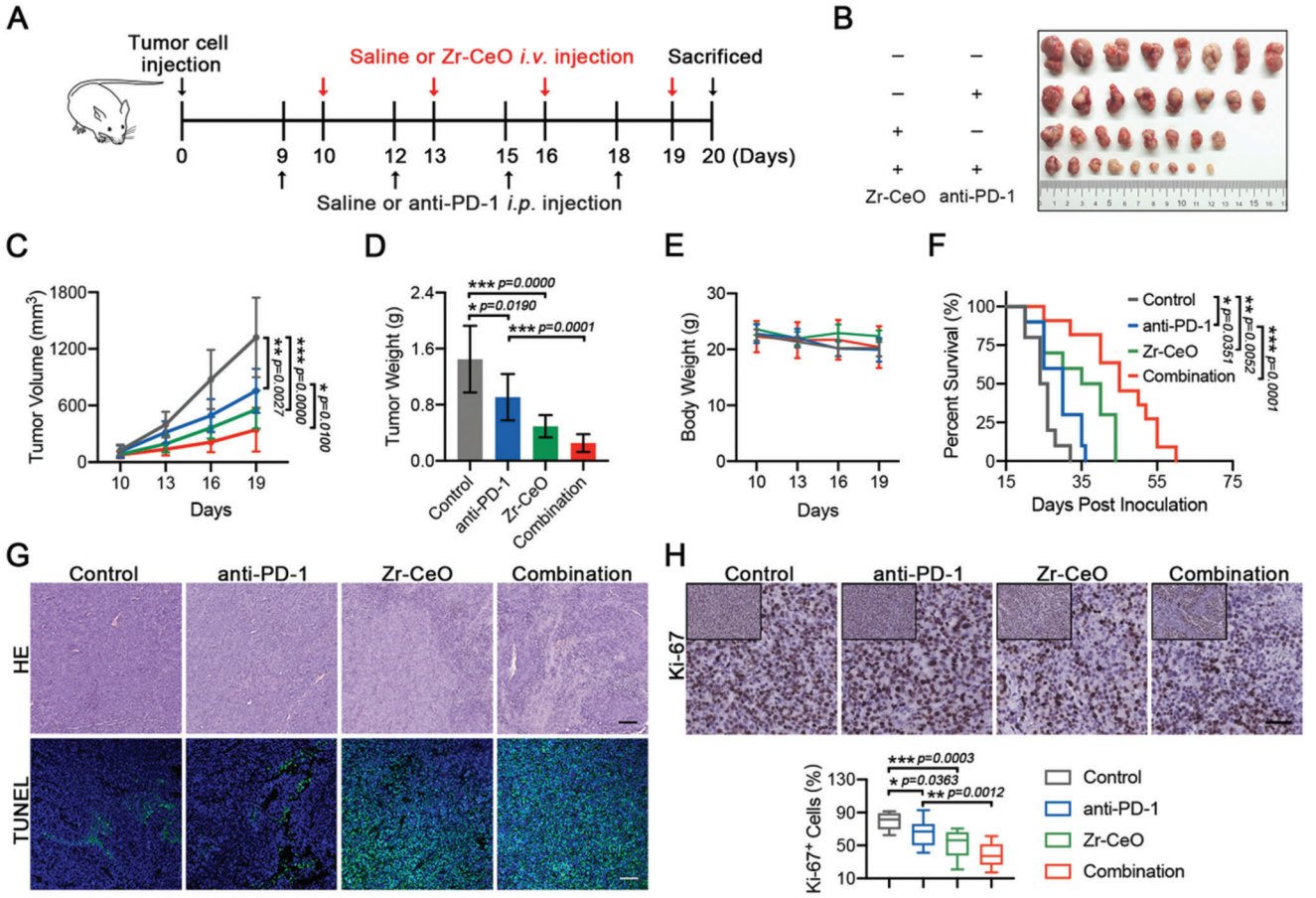

Figure 4. Zr-CeO enhanced the antitumor efficacy of PD-1 inhibition in renal subcutaneous tumors. A) Schematic illustration of the timeline for Renca subcutaneous tumor model establishment and cancer immunotherapy. Mice were assigned to four groups as follows: 1) saline; 2) anti-PD-1, 10 mg kg^{-1}; 3) Zr-CeO, 10 mg kg^{-1}; 4) combination ($n = 8$). B) Photograph of dissected Renca subcutaneous tumors at the endpoint. C) Sizes of tumors since first administration. D) Endpoint tumor weight in grams. E) Body weight of mice since first administration. F) Survival percentages of mice receiving different treatments ($n = 10$). G) Representative H&E and TUNEL staining of endpoint tumor sections. Scale bar: 100 μm. H) Representative immunohistochemistry staining for Ki-67 in endpoint tumor sections. Lower, quantification of the percentages of positive cells from eight high-power fields per group. Scale bar: 50 μm. Data in (C)–(E) are presented as mean ± SD. Data in (H) are shown as min to max. Statistical significance in (C) and (E) was evaluated using two-way ANOVA with Tukey's test. Statistical significance in (F) was evaluated using log-rank test. Statistical significance in (D) and (H) was evaluated using two-tailed Student's *t*-test. $^{*}p < 0.05$, $^{**}p < 0.01$, $^{***}p < 0.001$.

vs control: $p < 0.0001$; combination vs anti-PD-1: $p = 0.0001$; combination vs Zr-CeO: $p = 0.0050$) (Figure 4B–D), and mice almost maintained body weight during treatment (Figure 4E).

Clinically, anti-PD-1 alone or combined with a vascular endothelial growth factor receptor inhibitor showed benefits in advanced RCC with a significantly longer median overall survival or progression-free survival.[2a,d] We therefore evaluated the survival outcome for the Zr-CeO and anti-PD-1 combination treatment. Encouragingly, we observed a significant increase in survival compared to anti-PD-1 alone (45 days vs 30 days, $p = 0.0001$) or control group (45 days vs 25 days, $p < 0.0001$) (Figure 4F). Immunohistochemical data showed that combination treatment decreased the proportion of Ki-67 positive cells from 78.85% to 38.90% in cancer tissues, while anti-PD-1 group remained 65.16% (Figure 4H). Besides, the number of apoptotic cancer cells was immensely increased in Zr-CeO alone and combination treatment groups (Figure 4G). The above results demonstrate that the combination of Zr-CeO nanozyme and anti-PD-1 immunotherapy inhibits tumor growth in a renal carcinoma mouse model.

2.8. Zr-CeO Nanozyme-Enhanced Immunotherapy is Associated with TME Remodeling

We further examined the myeloid immunosuppressive cells to determine whether the antitumor effect of Zr-CeO and anti-PD-1 combination therapy was associated with a more immunogenic TME. The frequency of tumor-infiltrated MDSCs and M2 macrophages was analyzed by flow cytometry and immunohistochemistry. As shown in **Figure 5**A, G-MDSCs infiltration was significantly decreased after Zr-CeO treatment, compared to control or anti-PD-1 group (8.51% with Zr-CeO vs 18.27% with saline, $p = 0.0011$; 8.51% with Zr-CeO vs 14.10% with anti-PD-1, $p = 0.0071$). Both MDSC subtypes were sharply diminished in the TME of tumor-bearing mice with Zr-CeO and anti-PD-1 combi-

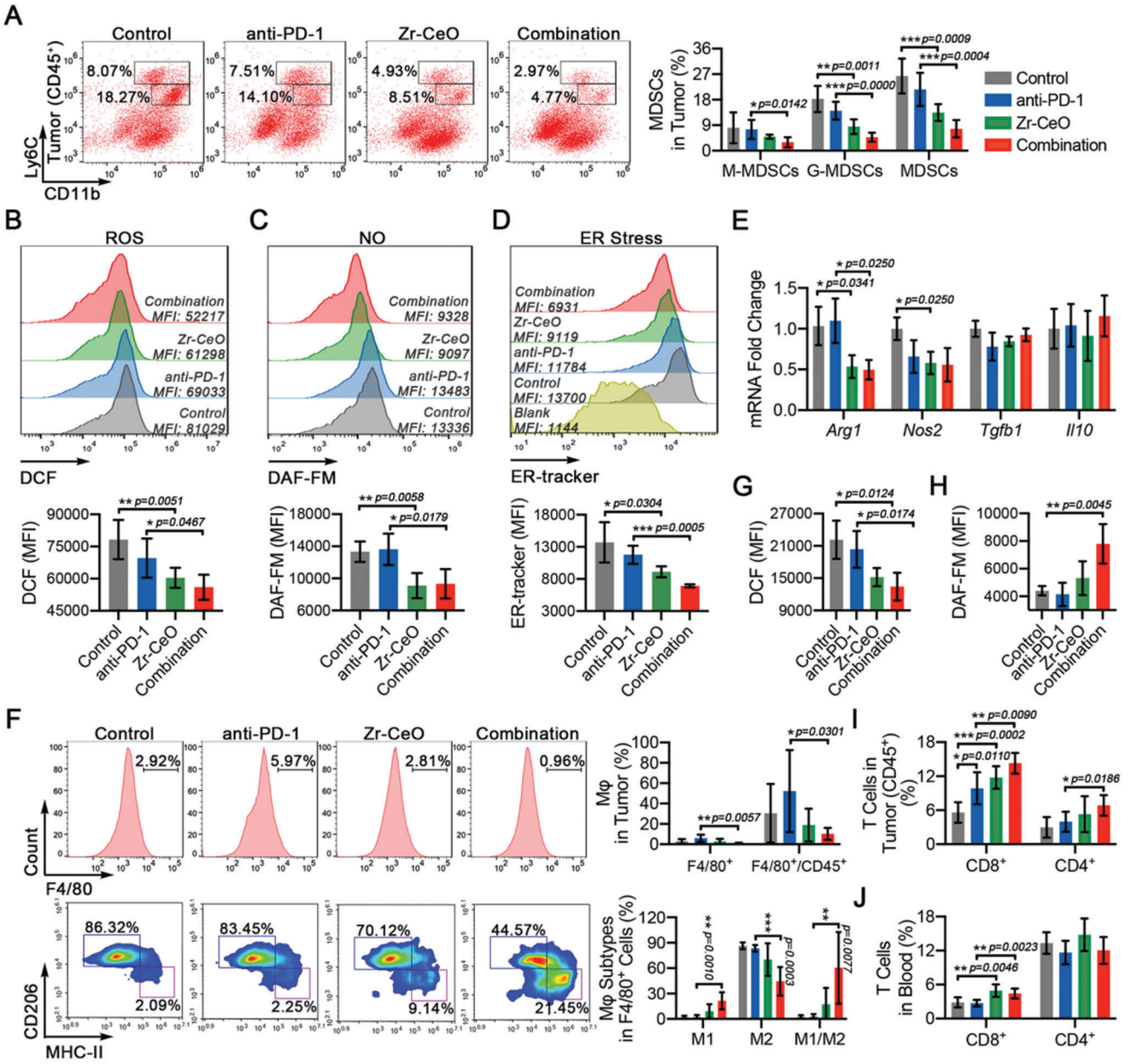

Figure 5. Zr-CeO-enhanced immunotherapy is associated with TME remodeling. A) Representative flow cytometry plots of $CD11b^+Ly6C^{high}$ M-MDSCs and $CD11b^+Ly6C^{low}$ G-MDSCs gating on $CD45^+$ cells in Renca tumors at the endpoint. Right, quantification of the percentages of MDSCs among $CD45^+$ cells ($n = 6$). B–D) Flow cytometric analysis of ROS, NO, and ER-tracker staining in Gr-1^+ MDSCs isolated from tumors with different treatments. Lower, quantification of the corresponding MFI ($n = 4$). E) RT-qPCR analysis of *Arg1*, *Nos2*, *Tgfb1*, and *Il10* levels in isolated Gr-1^+ MDSCs. F) Representative flow cytometry plots of $F4/80^+$ macrophages, $MHC\text{-}II^+CD206^-$ M1 and $MHC\text{-}II^-CD206^+$ M2 macrophages gating on F4/80 in tumors from renal-tumor-bearing mice with different treatments at the endpoint. Upper right, quantification of the percentages of $F4/80^+$ macrophages among all tumor cells and $CD45^+$ cells; lower right, quantification of the percentages of $MHC\text{-}II^+CD206^-$ M1 and $MHC\text{-}II^-CD206^+$ M2 macrophages among $F4/80^+$ macrophages, and the ratio of M1 to M2 ($n = 6$). G,H) Quantification of the MFI of ROS and NO in isolated $F4/80^+$ macrophages ($n = 4$). I) Quantification of the percentages of $CD8^+$ and $CD4^+$ T cells among $CD45^+$ cells in tumors. J) Quantification of the percentages of $CD8^+$ and $CD4^+$ T cells in blood. Data are presented as mean ± SD. Statistical significance was evaluated using two-tailed Student's *t*-test. $^*p < 0.05$, $^{**}p < 0.01$, $^{***}p < 0.001$.

nation treatment. The reduced infiltration of MDSCs was further validated by the immunohistochemistry data (Figure S17, Supporting Information). Moreover, the frequency of peripheral blood and splenic MDSCs was also decreased in Zr-CeO alone or combination group (Figure S18, Supporting Information).

To determine whether nanozyme and anti-PD-1 combination treatment attenuates the function of these infiltrated MDSCs, we utilized magnetic beads to isolate tumor Gr-1^+ MDSCs (Figure S19, Supporting Information) and measured the intracellular levels of ROS and NO. We found that infiltrated MDSCs in

nanozyme or combination group exhibited diminished intracellular ROS and NO (Figure 5B,C), as well as downregulated fluorescence of ER-tracker (Figure 5D). Both TME MDSCs following Zr-CeO or combination treatment had decreased levels of *Arg1* and *Nos2*, whereas no change was observed in the levels of *Tgfb1* and *Il10*, respectively (Figure 5E). These results suggest that Zr-CeO alone or combined with anti-PD-1 not only diminished MDSCs infiltration in the TME of renal-tumor-bearing mice but also influenced the expression of arginase 1 and iNOS of these MDSCs via ROS scavenging, which further confirmed the above in vitro data.

Meanwhile, we also observed a decrease in the infiltrated population of F4/80$^+$ TAMs accompanied with a substantial increase in the ratio of MHC-II$^+$CD206$^-$ M1 over MHC-II$^-$CD206$^+$ M2 macrophages in combination group compared with anti-PD-1 alone group (Figure 5F and Figure S20, Supporting Information), suggesting that combination treatment at least effectively reduced M2-TAM infiltration in vivo. Similarly, F4/80$^+$ TAMs were isolated from tumor tissues with distinct treatments, and the intracellular levels of ROS and NO were examined. ROS in TAMs was decreased following Zr-CeO and combination treatments as expected (Figure 5G and Figure S21A, Supporting Information), whereas NO was increased in contrast to the data of MDSCs (Figure 5H and Figure S21B, Supporting Information), potentially resulting from the Zr-CeO-induced repolarization toward the M1 subtype with elevated iNOS levels.

Reinforced antitumor T cell response indicates the success of ICB therapy. In the current study, we observed that anti-PD-1 or Zr-CeO treatment alone increased the frequency of tumor-infiltrating lymphocytes (TILs), in which CD8$^+$ T cells significantly expanded. Moreover, the combination treatment showed obvious accumulation of both CD4$^+$ and CD8$^+$ TILs, compared to anti-PD-1 group (Figure 5I and Figures S22 and S23, Supporting Information). In addition, periphery blood CD8$^+$ T cells also increased following Zr-CeO or combination treatment, but CD4$^+$ T cells barely changed (Figure 5J and Figure S24, Supporting Information). Immunohistochemistry analysis showed the elevated levels of IFN-γ in Zr-CeO or combination treatment in tumor tissues (Figure S25, Supporting Information), suggesting the enhancement of CD8$^+$ T cell response induced by nanozyme in renal TME. In addition, although ccRCC is highly infiltrated with CD8$^+$ T cells, the abundant CD8$^+$ TILs are functionally and metabolically impaired because they have small, fragmented mitochondria that generate large amounts of ROS.[33] Apart from indirect ways, scavenging mitochondria ROS in CD8$^+$ TILs may partially restore TIL activation directly. Although the particular role of Zr-CeO nanozyme on CD8$^+$ TIL activation needs further investigation, Zr-CeO and anti-PD-1 combination therapy indeed reinvigorated an effective antitumor immune response associated with TME remodeling.

2.9. Zr-CeO Nanozyme Enhanced Anti-PD-1 Efficacy in Triple-Negative Breast Cancer (TNBC)

To expand the above observations in a different cancer type, we used the murine 4T1 cell line, which exhibits the characteristics of human TNBC subtype, for further investigation. Compared with RCC, TNBC has lower responses to ICB monotherapies, among 3–18.5%.[3c,34] Moreover, the approval for atezolizumab (anti PD-L1) was withdrawn in 2021 due to the negative data from Mpassion131 (i.e., combining atezolizumab with paclitaxel did not improve progression free survival or overall survival vs paclitaxel alone).[35] To date, only pembrolizumab (anti PD-1) and chemotherapy combination therapy has been approved for previously untreated locally recurrent inoperable or metastatic TNBC.[35a] Similar to renal cancer, Zr-CeO with various concentrations barely changed the viability and apoptosis of 4T1 cells in vitro (Figure S26, Supporting Information). We subsequently explored the role of Zr-CeO and anti-PD-1 combination therapy in an orthotropic Balb/c murine mammary tumor model. Consistent with the clinical data, PD-1 inhibition (10 mg kg^{-1}) had a minor effect on breast tumor growth (**Figure 6**A) and barely affected the survival outcome (Figure 6D). In contrast, compared with anti-PD-1 group, the combination group showed significantly better effects on tumor growth inhibition (Figure 6A,B) as well as extension of survival (Figure 6D) without large weight fluctuation (Figure 6C). Both Zr-CeO alone and combination treatment decreased proliferation and increased apoptosis (Figure 6E). Furthermore, the enhanced antitumor effects of Zr-CeO alone and combination treatment in breast cancer were accompanied with a reduced population of MDSCs in the TME and spleen (Figure 6F and Figure S27, Supporting Information) and an increase in the M1/M2 ratio (Figure 6G and Figure S28A, Supporting Information). However, both treatments barely influenced the frequency of total TAMs (Figure 6G and Figure S28, Supporting Information). Correspondingly, the antitumor immune response was also strengthened in breast tumors and peripheral immune organs undergoing Zr-CeO alone and combination treatment. The frequency of CD8$^+$ T cells approximately doubled in breast tumors, with an observable enhancement of IFN-γ levels (Figure 6H and Figures S29 and S30, Supporting Information), while the number of infiltrated CD4$^+$ T cells barely changed (Figure 6I and Figure S31, Supporting Information). Together, our data revealed the effect of Zr-CeO nanozyme on tumor growth inhibition and TME modulation, which was consistent with renal cancer. Combined, the efficacy toward the two tumor models demonstrated Zr-CeO as a promising adjuvant quite possibly applicable to other tumors abundantly infiltrated with myeloid suppressive cells to potentiate immunotherapy in the clinic.

3. Conclusions

In summary, we developed Zr-CeO nanozyme with enhanced SOD-like and CAT-like activities, and employed it to successfully inhibit renal tumor growth. The nanozyme was rapidly distributed in major organs and could reside in tumors for at least 48 h with favorable in vivo biosafety. Zr-CeO nanozyme had no direct effect on the growth status of cancer cells and marginally influenced CAFs, but simultaneously reversed MDSC immunosuppression and M2-TAM polarization by eliminating intracellular ROS. Specifically, in MDSCs, Zr-CeO-induced ROS scavenging dampened UPR, downregulated arginase 1 and iNOS transcriptionally, and therefore enhanced T cell proliferation. In macrophages, the nanozyme hindered M2-TAM polarization via suppressing ERK and STAT3 pathways. Furthermore, as demonstrated in murine renal and breast tumor models, the Zr-CeO nanozyme in combination with PD-1 antibody showed

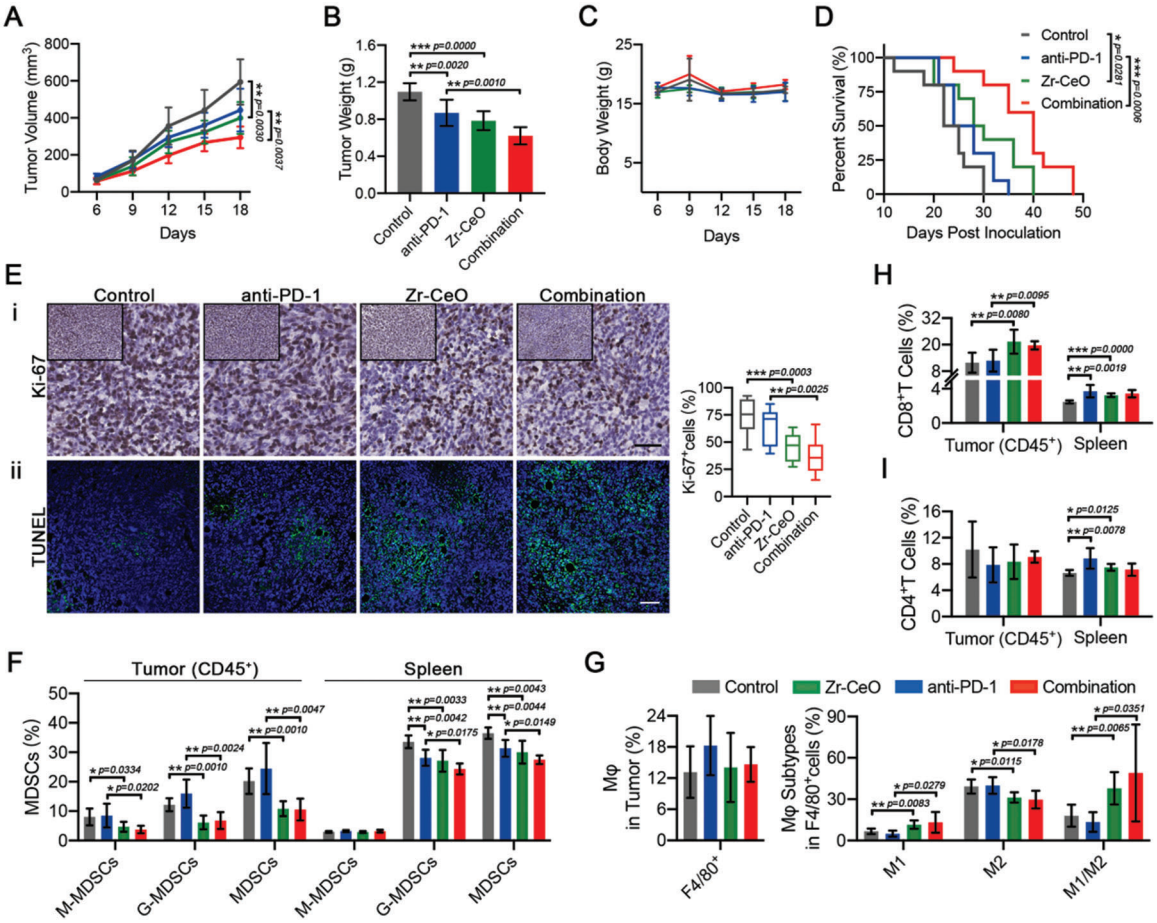

Figure 6. Zr-CeO enhanced anti-PD-1 efficacy in TNBC. A) Sizes of dissected orthotopic 4T1 tumors from mice with different treatments consistent with Figure 4 ($n = 8$). B) Endpoint tumor weight in grams. C) Body weight of mice since first administration. D) Survival percentages of mice receiving different treatments ($n = 10$). E) i) Representative immunohistochemistry staining for Ki-67 in endpoint tumor sections. Scale bar: 50 μm. Right, quantification of the percentages of positive cells from eight high-power fields per group; ii) Representative TUNEL staining of endpoint tumor sections. Scale bar: 100 μm. F) Quantification of the percentages of MDSCs and the subpopulations in tumors (gated on $CD45^+$) and spleens from breast-tumor-bearing mice ($n = 6$). G) Quantification of the percentages of $F4/80^+$ macrophages among all tumor cells, M1 and M2 macrophages among $F4/80^+$ macrophages, and the ratio of M1 to M2. H,I) Quantification of the percentages of $CD8^+$ and $CD4^+$ T cells in tumors (gated on $CD45^+$) and spleens. Data in (A–C) and (F–I) are presented as mean ± SD. Data in (E) are shown as min to max. Statistical significance in (A) and (C) was evaluated using two-way ANOVA with Tukey's test. Statistical significance in (D) was evaluated using log-rank test. Statistical significance in (B) and (E–I) was evaluated using two-tailed Student's *t*-test. $*p < 0.05$, $**p < 0.01$, $***p < 0.001$.

superior efficiency in tumor growth inhibition associated with an enhanced antitumor immune response. This study elaborates the dual effects of Zr-CeO in TME remodeling, providing a facilely designed nanoparticle with a strong capacity to manipulate the quantity and function of immunosuppressive myeloid cells as a new strategy to sensitize clinical ICB therapy in more than one cancer types.

4. Experimental Section

Reagents and Antibodies: $Ce(NO_3)_3{\cdot}6H_2O$ (cerium nitrate hexahydrate) and $ZrO(NO_3)_2{\cdot}xH_2O$ (zirconium oxynitrate hydrate) were obtained from Aladdin (Shanghai, China). Ethylene glycol (98%), ammonia solution (25–28%), citric acid monohydrate, sodium citrate dihydrate, and H_2O_2 (hydrogen peroxide, 30%) were purchased from Sinopharm Chemical Reagent Ltd. (Shanghai, China). SOD Assay Kit-WST was obtained from Dojindo (Tokyo, Kumamoto, Japan). Anti-mouse PD-1 antibody was provided by Shanghai Junshi Biosciences Co., Ltd. Antibodies for Ki-67, CD206, vimentin, arginase-1, STAT3, phospho-STAT3 (Tyr705), and tubulin were purchased from Cell Signaling Technology (Boston, MA, USA). Antibodies for IFN-γ and phospho-PERK (Thr981) were purchased from Immunoway (Plano, Texas, USA). Antibodies for CD8α, α-SMA, and F4/80 were purchased from Abcam (Boston, MA, USA). Antibodies for E-cadherin, PERK, IRE1, ERK 1/2, iNOS, GAPDH, and β-actin were purchased from Proteintech (Rosemont, NJ, USA). Antibodies for CD3, CD28, Gr-1, and phospho-IRE1α (Ser724) were purchased from Invitrogen (Carlsbad, CA, USA). Antibody for phospho-ERK 1/2 (T202) was from Bioworld (St. Louis Park, MN, USA). Antibody for CD4 was purchased from Santa Cruz Biotechnology (Delaware, CA, USA). Anti-mouse antibodies for PerCP/cy5.5-CD45, APC-F4/80, PE-Gr-1, PE-Ly6C, FITC-CD206, PerCP/cy5.5-CD206, and APC-CD8α were purchased from Biolegend (San Diego, CA, USA). Anti-mouse FITC-CD11b antibody was purchased from BD Pharmingen (San Diego, CA, USA). Anti-mouse antibodies for FITC-CD4 and PE-MHC-II were purchased from Invitrogen. All other reagents and chemicals were purchased from commercial sources and used as received.

Instrumentation: TEM images were obtained from a JEM-2800 (JEOL, Tokyo, Japan) at an acceleration voltage of 200 kV. FT-IR spectra were recorded on a spectrometer (Perkin Elmer, Waltham, MA, USA). XRD patterns were collected on a D8 Advance (Bruker, Karlsruhe, GER). XPS spectra were collected on an ESCALAB250Xi (Thermo Fisher Scientific, Waltham, MA, USA). Absorbance was recorded on a SpectraMax M2e microplate reader (Molecular Device, Sunnyvale, CA, USA). DLS and zeta potential results were measured by Zetasizer NanoZSP (Malvern, Worcestershire, UK). The generated dissolved oxygen was measured by SevenExcellence (Mettler Toledo, Switzerland).

Preparation of Zr-CeO NPs: The Zr-CeO NPs were synthesized as described earlier with modification.[36] Typically, $Ce(NO_3)_3$ (252 mg) and $ZrO(NO_3)_2$ (155 mg) were dissolved into an equal proportion mixture of ethylene glycol and water (20 mL) to form a clear solution. After the injection of ammonia water (25–28%, 4 mL), the obtained solution was incubated at 60 °C for 3 h under vigorous stirring. During the stirring process, the color of the reaction system turned from purple to yellow. Finally, after centrifugation (11 000 rpm, 10 min) and washing (three times, water/ethanol), the CeZrO NPs were obtained. The modification was first carried out by the dropwise addition of citric acid (60 mg mL^{-1}, 5 mL) and centrifugation (8000 rpm, 10 min). Then, sodium citrate (60 mg mL^{-1}, 5 mL) was added to the precipitate to obtain the modified Zr-CeO.

Preparation of CeO NPs: The preparation of CeO NPs followed the same protocol as Zr-CeO NPs in the absence of $ZrO(NO_3)_2$.

CAT-Like Activity of Zr-CeO NPs: The CAT-like activity of Zr-CeO NPs was evaluated by the amount of generated oxygen via a dissolved oxygen meter. Typically, CeO or Zr-CeO NPs (100 µg mL^{-1}) and a detector of dissolved oxygen meter were added to the H_2O_2 solution (1×10^{-3} M) simultaneously. The concentration of dissolved oxygen was recorded during the following 30 min to determine the CAT-like activity.

SOD-Like Activity of Zr-CeO NPs: The SOD-like activity of Zr-CeO NPs was determined by a SOD assay kit (Dojindo). In this assay, xanthine and xanthine oxidase were applied to generate superoxide anions, and WST-1 was used as a specific probe. First, the enzyme and WST-1 working solution was diluted according to the manufacturer's protocols. Then, CeO or Zr-CeO NPs (20 µL, final concentrations: 2.5, 5, 10, and 20 µg mL^{-1}) and enzyme working solution (20 µL) were added to the WST-1 working solution (200 µL). After incubation at 37 °C for 20 min, the absorbance at 450 nm was determined. The SOD-like activity of Zr-CeO NPs was determined by the scavenging rate of the superoxide anions.

Cell Lines and Treatments: All cells were routinely cultured in a humidified incubator with a constant temperature of 37 °C in 5% CO_2. HK-2 (human renal proximal tubular epithelial cell line), 769P (human ccRCC line), and ACHN (human RCC line) were obtained from the Cell Bank of the Chinese Academy of Sciences (Shanghai). Renca (murine RCC line) and 4T1 (murine mammary carcinoma line) were purchased from the American Type Culture Collection (Rockville, MD, USA). HK-2 and ACHN cells were maintained in Dulbecco's modified Eagle medium (Sigma-Aldrich, Darmstadt, GER), while 769P, Renca, and 4T1 cells were maintained in RPMI-1640 medium (Sigma-Aldrich), both supplemented with 10% fetal bovine serum (FBS, Thermo Fisher Scientific) and 1% penicillin-streptomycin (10 000 U mL^{-1}, Thermo Fisher Scientific). The above cells were further treated with saline or Zr-CeO (2.5, 10, or 20 µg mL^{-1}) and collected at different times for various assessments.

Induction and Treatments of MDSCs and Macrophages: BM-MDSCs and BMDMs were obtained from Balb/c mice as previously reported.[37] Briefly, bone marrow cells (BMs) were planted into plates using RPMI-1640 medium with 10% FBS, 1% penicillin-streptomycin, 40 ng mL^{-1} IL-6 (StemCell, Vancouver, WA, USA), and 40 ng mL^{-1} GM-CSF (PeproTech, Rocky Hill, NJ, USA) for 4 days to induce MDSCs. Then, saline or Zr-CeO (2.5, 5, or 10 µg mL^{-1}) were added to BM-MDSCs 48 h before collection. In addition, BMDMs were also induced with 40 ng mL^{-1} M-CSF (PeproTech). After 7 days, the differentiated BMDMs were co-cultured with 20 ng mL^{-1} IL-4 (StemCell) plus saline or plus Zr-CeO (2.5, 10, or 20 µg mL^{-1}) for 24 h. To induce TAMs in vitro, THP-1 (human leukemia monocytic cell line) cells, obtained from the Cell Bank of the Chinese Academy of Science, were resuspended in RPMI-1640 medium with 10% FBS and seeded in 12-well plates (1.5×10^5 cells per well). After treatment with phorbol 12-myristate 13-acetate (PMA, 50×10^{-9} M, Sigma-Aldrich) for 12 h, the adherent cells became M0 macrophages. Subsequently, these PMA-induced M0 macrophages were co-cultured with the renal cancer cell line ACHN (2.0×10^5 cells per well) cells for 72 h and treated with saline or Zr-CeO (2.5, 10, or 20 µg mL^{-1}) for the same duration.

Isolation and Treatments of RCC-Associated Fibroblasts and Normal Fibroblasts: Renal tissues were obtained from patients undergoing renal tumor resection in Nanjing Drum Tower Hospital. The acquisition of tissues was in accordance with the Declaration of Helsinki and approved by the Ethics Committee of Nanjing Drum Tower Hospital (2021-582-01). CAFs and NFs were isolated from three pairs of fresh renal cancer tissues and paired normal renal tissues, respectively. The fresh tissues were minced and digested in DMEM medium containing 1.5 mg mL^{-1} collagenase IV (Gibco, Carlsbad, CA, USA) and 250 µg mL^{-1} hyaluronidase (Sigma-Aldrich) under rotation at 37 °C for 1 h. Then, the digested tissue pieces were inoculated in DMEM/F12 supplemented with 10% FBS and 1% penicillin-streptomycin. After the supernatant was removed on the 3rd day, the adherent cells were mostly fibroblasts. To obtain purer fibroblasts, the cells were cultured for another 3 days and replaced with fresh medium every day. Both CAFs and NFs were co-cultured with saline or Zr-CeO (2.5, 5, 10, or 20 µg mL^{-1}) for immunofluorescence or cell viability assay.

Cytotoxicity and Apoptosis Assay: A CCK-8 kit (Vazyme Biotech, Nanjing, Jiangsu, China) was used to analyze the cytotoxicity of Zr-CeO on renal cancer cells, breast cancer cells, and IL-4-induced M2 macrophages according to the manufacturer's instructions. In brief, after treatment with Zr-CeO, cells in 96-well plates were co-cultured with CCK-8 (10 ×) and incubated at 37 °C for 2 h. The absorbance was detected at 450 nm with a reference wavelength at 650 nm. A Cell Cycle and Apoptosis Detection Kit (YEASEN, Shanghai, China) was used to analyze the apoptosis of renal cancer cells, breast cancer cells, and BM-MDSCs as manufactory's protocol. Briefly, after washing with precooled phosphate-buffered saline (PBS), the collected cells were resuspended in binding buffer containing Annexin V and propidium iodide (PI). After 15 min of reaction in the dark, the samples were detected by using a flow cytometer.

$CD8^+$ T Cells Proliferation Assay: $CD8^+$ T cells were enriched using an EasySep Mouse $CD8^+$ T Cell Isolation Kit (StemCell) from the spleens of 8 weeks old male Balb/c mice according to the instructions. Specifically, the spleens of Balb/c mice were sheared and passed through a 70 µm cell strainer. After red blood cells were depleted, the remaining cells were resuspended in sorting buffer (PBS containing 2% FBS and 1×10^{-3} M ethylenediaminetetraacetic acid (EDTA)) and incubated with rat serum and isolated cocktail for 10 min. Then, the magnetic beads were added and incubated for 5 min, and the tube was placed in a magnetic rack. Another 5 min later, the supernatant poured out was mostly $CD8^+$ T cells. These $CD8^+$ T cells were then centrifuged, washed, and co-cultured with 5,6-carboxyfluorescein diacetate succinimidyl ester (CFSE) proliferation dye (Invitrogen) for 15 min in the dark at 37 °C. After washing with PBS, the cells were resuspended in RPMI-1640 medium supplemented with anti-mouse CD28 antibody (1 µg mL^{-1}) and 10% FBS and seeded into a 96-well plate precoated with anti-mouse CD3 antibody (1 µg mL^{-1}). Subsequently, they were divided into three groups: 1) $CD8^+$ T cells treated with different concentrations of Zr-CeO; 2) $CD8^+$ T cells co-cultured with MDSCs that were pretreated with different concentrations of Zr-CeO for 48 h; 3) $CD8^+$ T cells co-cultured with MDSCs and different concentrations of Zr-CeO simultaneously (MDSCs, 1×10^4 cells per well; $CD8^+$ T cells, 4×10^4 cells per well). 72 h later, the cells were collected, washed, and blocked with 1% bovine serum albumin (BSA, Sigma-Aldrich) for 30 min at 4 °C. After incubating with an APC-conjugated anti-mouse CD8 antibody for another 30 min, the cells were subjected to flow cytometry to measure the proliferation level of $CD8^+$ T cells.

Murine Tumor Models and Treatments: 7 to 8 weeks old Balb/c mice were purchased from GemPharmatech Co., Ltd. (Nanjing, Jiangsu, China). All animal experiments were carried out according to the National Institutes of Health Guide for the Care and Use of Laboratory Animals and approved by the Ethics Committee of Nanjing Drum Tower Hospital (2021AE01059). To establish a renal tumor model, each Balb/c male mouse was subcutaneously inoculated with 5×10^5 Renca cells in the right hind limb. For orthotopic models of TNBC, each Balb/c female mouse was

inoculated with 2.5×10^5 4T1 cells into the fourth mammary fat pad on the right. Tumor volume, mouse body weight, and status were measured and recorded. Tumor length and width were measured by a Vernier caliper once every 3 days with the calculation formula as follows: Tumor volumes = length × width^2/2. Mice were grouped for treatments when the tumor volume reached 50–100 mm^3. To explore the therapeutic effect of Zr-CeO in renal cancer, mice were randomly divided into two groups and intravenously injected with saline (control) or nanozyme (Zr-CeO, 10 mg kg^{-1}) on day 12, followed by every 3rd day of treatment until the experimental endpoint ($n = 6$ per group). To determine the efficacy of Zr-CeO combined with immunotherapy in renal or breast tumors, mice were assigned to four groups ($n = 8$ per group) as follows: 1) control, saline, i.v. and i.p.; 2) anti-PD-1, 10 mg kg^{-1}, i.p.; 3) Zr-CeO, 10 mg kg^{-1}, i.v.; 4) combination, 10 mg kg^{-1} anti-PD-1 antibody and 10 mg kg^{-1} Zr-CeO, respectively. Zr-CeO treatment was provided 1 day after anti-PD-1 injection, and each treatment was repeated every 3 days until sacrifice. For biodistribution exploration, mice with Renca subcutaneous tumor around 140 mm^3 were intravenously injected with 10 mg kg^{-1} Zr-CeO. The hearts, livers, spleens, lungs, kidneys, and tumors were collected at 3, 12, 24, and 48 h ($n = 3$ per time point) and digested with aqua regia, followed by utilizing ICP-MS to determine the content of zirconium. To observe the short-term toxicity of Zr-CeO on major organs, male 8 weeks old Balb/c mice were injected i.v. with 10 mg kg^{-1} Zr-CeO. After 24 h, the hearts, livers, spleens, lungs, and kidneys were collected. For long-term biosafety examination, mice were injected i.v. with 10 mg kg^{-1} Zr-CeO once every 3 days, and the collected organs were subjected to H&E staining to assess pathological toxicity. To further evaluate the effect of Zr-CeO on blood biochemical indexes, healthy mice were injected i.v. with a series dose of Zr-CeO (0, 5, 10, 20 mg kg^{-1}). After 24 h (single injection) or 12 days (once every 3 days), the blood samples were collected and the serum was separated ($n = 3$). The levels of creatinine, blood urea nitrogen (BUN), alanine aminotransferase (ALT), aspartate transaminase (AST), and alkaline phosphatase (ALP) in serum were analyzed using the corresponding kits (Elabscience Biotechnology Co., Ltd., Wuhan, China) and detected by a M200 PRO microplate reader (TECAN, Switzerland) according to the manufacturer's instructions, respectively.

Preparation of Tumor MNCs: Tumor mononuclear cells (MNCs) were isolated and purified from renal and breast tumors. Tumors were cut into small fragments and digested with RPMI-1640 medium containing 1.0 mg mL^{-1} collagenase type I, 250 µg mL^{-1} hyaluronidase, and 100 U mL^{-1} DNase I (Vazyme Biotech) for 45 min at 37 °C. After passing through a 70 µm cell strainer, the cells were centrifuged at 400 × *g* for 10 min and resuspended with 40% Percoll (Cytiva, Washington DC, USA). Then, the cell suspension was slowly overlaid on 70% Percoll solution and centrifuged at 400 × *g* for 20 min at room temperature. Finally, the obtained cells in the intermediate layer were regarded as MNCs and washed with PBS for the magic cell sorting system (MACS) and flow cytometry analysis.

Isolation of MDSCs and Macrophages from Tumor MNCs: MDSCs were isolated from tumor-purified MNCs, magnetically labeled and positively selected according to the instructions provided by the MDSC Isolation Kit (Miltenyi Biotec, Bergisch Gladbach, GER). In brief, cells resuspended in sorting buffer (PBS containing 0.5% BSA, 2×10^{-3} M EDTA, pH 7.2) were incubated with FcR blocking reagent at 4 °C for 10 min and incubated with anti-Gr-1-Biotin at 4 °C for another 10 min. After washing with sorting buffer, the resuspended cells were incubated with anti-biotin microbeads for 15 min at 4 °C, centrifuged, and resuspended. The cells were subsequently applied onto the prerinsed columns in the magnetic separator to isolate Gr-1$^+$ MDSCs. For TAMs isolation, MNCs were resuspended with sorting buffer and incubated with anti-F4/80 microbeads (Miltenyi Biotec) at 4 °C for 15 min. After washing, the cell suspension was subjected to a magnetic separator to isolate F4/80$^+$ TAMs, similar to MDSCs. These positively separated MDSCs and macrophages were further identified by flow cytometry.

Flow Cytometry Analysis: Mice whole blood was collected using sterile 3.8% sodium citrate for anticoagulation and centrifuged to remove plasma. The lower cells were lysed to remove red blood cells and washed with PBS. For preparation of splenic cells, spleens were minced and gently rolled in PBS and filtered with a 70 µm cell strainer. After depletion of red blood cells, the remaining cells were washed with PBS. 5×10^5 cells from tumor MNCs, blood, and spleen were blocked with 1% BSA for 30 min at 4 °C and incubated with fluorescent antibodies or isotype antibodies at 4 °C for another 30 min. The intracellular ROS levels were detected by using a DCFH-DA probe (Beyotime, Haimen, Jiangsu, China), while nitric oxide (NO) levels were detected by a DAF-FM DA probe (Beyotime). Cells (1–20 million mL^{-1}) were resuspended with 10 µmol L^{-1} DCFH-DA or 5 µmol L^{-1} DAF-FM DA and then incubated at 37 °C for 20 min. For ER-tracker staining, cells were probed with 1×10^{-6} M ER-tracker red (YEASEN) and incubated at 37 °C for 30 min. Data acquisition was performed with a NovoCyte device (Agilent Technologies Inc., Santa Clara, CA, USA). All analysis was performed using FlowJo version 10 software.

H&E Staining, Immunohistochemistry, Immunofluorescence, and TUNEL: The above tumor tissues were fixed in 4% paraformaldehyde and embedded in paraffin. Paraffin blocks were sectioned to obtain 3 µm thick tissue samples, and the samples were deparaffinized, hydrated, and washed. After staining with H&E, the samples were viewed by a light microscope (Leica DM1000, Leica Biosystems Inc., Heerbrugg, GER). For immunohistochemistry, after antigen retrieval was performed, the samples were blocked with 5% BSA and incubated with anti-Ki-67, anti-Gr-1, anti-CD206, anti-CD8α, anti-CD4, or anti-IFN-γ antibodies overnight at 4 °C. The samples were then washed and incubated with the secondary antibody (Vector Laboratories, Burlingame, CA, USA) for 1 h at room temperature, stained with diaminobenzidine substrate (DAB, ORIGENE, Rockville, MD, USA), and observed with a light microscope (Leica DM1000). For immunofluorescence, slides seeded with NFs and CAFs were permeabilized with 0.3% Triton X-100 (SunShine Biotechnology Co., Nanjing, Jiangsu, China) for 30 min, blocked with 5% BSA for 1 h, and then incubated with anti-α-SMA, anti-vimentin, or anti-E-cadherin antibodies overnight at 4 °C and the respective fluorescence-labeled secondary antibodies (Invitrogen) at temperature for 1 h. After the nuclei of cells were stained with 4′,6-diamidino-2-phenylindole (DAPI, Beyotime) for 10 min, the samples were washed and observed using a fluorescence microscope (Leica DMi8, Leica Biosystems Inc.). TUNEL assay was performed using a TUNEL BrightGreen apoptosis detection kit (Vazyme Biotech). According to the steps provided by the manufacturer, the samples were permeabilized with 20 µg mL^{-1} proteinase K for 20 min, washed with PBS, and equilibrated with equilibration buffer for 30 min. After the equilibration solution was aspirated off, the samples were incubated with TdT incubation buffer (a mixture of 34 µL ddH_2O, 10 µL 5 × equilibration buffer, 5 µL BrightGreen labeling mix, and 1 µL recombinant TdT enzyme) at 37 °C for 60 min. The samples were then stained with DAPI for 10 min and mounted with 20% glycerol. Observation was performed with a fluorescence microscope (Leica DMi8).

Western Blot: MDSCs and macrophages were washed with PBS, and total protein was extracted from the cells by using cell lysates (Beyotime) containing phosphatase inhibitors (Thermo Fisher Scientific) and protease inhibitors (Thermo Fisher Scientific) for incubation on ice for 30 min. After centrifugation at 12 000 *g* for 10 min, the supernatant was collected and the protein concentration was determined with a BCA kit (Beyotime). Protein expression was analyzed by western blot. Protein extracts were separated by 10% sodium dodecyl sulfate polyacrylamide gel electrophoresis and transferred to polyvinylidene fluoride membranes. After blocking with 5% nonfat milk in PBS containing 0.1% Tween-20, the membranes were incubated with primary antibodies against arginase 1, iNOS, phospho-PERK (Thr981), PERK, phospho-IRE1, IRE1, phospho-ERK 1/2 (T202), ERK, phospho-STAT3 (Tyr705), STAT3, β-actin, GAPDH, or tubulin at 4 °C overnight. After washing, the membranes were incubated with respective secondary antibodies (Santa Cruz Biotechnology) at room temperature for 1 h. The membranes were then incubated with electrochemiluminescence substrate (ECL, Vazyme), and the expression levels of proteins were visualized using a chemiluminescence imager (Clinx Science Instruments Co., Shanghai, China).

Quantitative Reverse Transcription Polymerase Chain Reaction (RT-PCR): Total RNA of MDSCs and macrophages was extracted with TRIzol reagent (Invitrogen) according to the manufacturer's protocol. For RNA quantification, 1 µg of total RNA was reversely transcribed into cDNA with PrimeScriptRT master mix (Takara, Tokyo, Japan). The reaction was performed at 37 °C for 15 min and 85 °C for 5 s. For quantitative RT-PCR

(RT-qPCR), cDNA, SYBR Premix Ex Taq (Takara), and specific primers were used. The sequences of the primers are listed in Table S1 in the Supporting Information. All primers were synthesized by Generay Biotech (Shanghai) Co., Ltd. The reaction condition was at 95 °C for 5 min, and then 40 cycles of 95 °C for 10 s and 60 °C for 30 s. Cycle threshold (CT) values were set with a fixed threshold, and the expression of relevant mRNAs was normalized with β-actin. The numerical formula is $2^{-\Delta\Delta CT}$, $\Delta\Delta CT = (C_{T\ mRNA} - C_{T\ \beta\text{-actin}})_{\ target} - (C_{T\ mRNA} - C_{T\ \beta\text{-actin}})_{\ control}$.

Statistical Analysis: All data were analyzed with GraphPad Prism V9. Sample size (n) for each statistical analysis was individually specified in the corresponding legend. The data were represented as min to max in immunohistochemistry graphs and as mean ± SD everywhere else. Two-sample comparisons were performed using two-tailed Student's t-test. Data of tumor growth and body weight were analyzed via analysis of variance (ANOVA) with Tukey's test. Survival curves were analyzed by log-rank test. $*p < 0.05$, $**p < 0.01$, $***p < 0.001$ were considered statistically significant.

Supporting Information

Supporting Information is available from the Wiley Online Library or from the author.

Acknowledgements

W.M., S.L., and X.Z. contributed equally to this work. The work was supported by grants from the National Natural Science Foundation of China (81972388 to H.G., 82173160 to W.D., 82070703 and 92168112 to X.Z.); the National Key R&D Program of China (2021YFF1200700 and 2019YFA0709200 to H.W.) and the China Postdoctoral Science Foundation (2019M661808 to W.D.).

Conflict of Interest

The authors declare no conflict of interest.

Data Availability Statement

The data that support the findings of this study are available from the corresponding author upon reasonable request.

Keywords

cancer immunotherapy, immune checkpoint blockade therapy, myeloid-derived suppressor cells, nanozymes, tumor-associated macrophages

Received: January 18, 2023
Revised: March 24, 2023
Published online:

[1] Y. Senbabaoglu, R. S. Gejman, A. G. Winer, M. Liu, E. M. Van Allen, G. de Velasco, D. Miao, I. Ostrovnaya, E. Drill, A. Luna, N. Weinhold, W. Lee, B. J. Manley, D. N. Khalil, S. D. Kaffenberger, Y. Chen, L. Danilova, M. H. Voss, J. A. Coleman, P. Russo, V. E. Reuter, T. A. Chan, E. H. Cheng, D. A. Scheinberg, M. O. Li, T. K. Choueiri, J. J. Hsieh, C. Sander, A. A. Hakimi, *Genome Biol.* **2016**, *17*, 231.

[2] a) T. K. Choueiri, T. Powles, M. Burotto, B. Escudier, M. T. Bourlon, B. Zurawski, V. M. Oyervides Juarez, J. J. Hsieh, U. Basso, A. Y. Shah, C. Suarez, A. Hamzaj, J. C. Goh, C. Barrios, M. Richardet, C. Porta, R. Kowalyszyn, J. P. Feregrino, J. Zolnierek, D. Pook, E. R. Kessler, Y. Tomita, R. Mizuno, J. Bedke, J. Zhang, M. A. Maurer, B. Simsek, F. Ejzykowicz, G. M. Schwab, A. B. Apolo, et al., *N. Engl. J. Med.* **2021**, *384*, 829; b) B. I. Rini, E. R. Plimack, V. Stus, R. Gafanov, R. Hawkins, D. Nosov, F. Pouliot, B. Alekseev, D. Soulieres, B. Melichar, I. Vynnychenko, A. Kryzhanivska, I. Bondarenko, S. J. Azevedo, D. Borchiellini, C. Szczylik, M. Markus, R. S. McDermott, J. Bedke, S. Tartas, Y. H. Chang, S. Tamada, Q. Shou, R. F. Perini, M. Chen, M. B. Atkins, T. Powles, K. Investigators, *N. Engl. J. Med.* **2019**, *380*, 1116; c) R. J. Motzer, K. Penkov, J. Haanen, B. Rini, L. Albiges, M. T. Campbell, B. Venugopal, C. Kollmannsberger, S. Negrier, M. Uemura, J. L. Lee, A. Vasiliev, W. H. Miller, Jr., H. Gurney, M. Schmidinger, J. Larkin, M. B. Atkins, J. Bedke, B. Alekseev, J. Wang, M. Mariani, P. B. Robbins, A. Chudnovsky, C. Fowst, S. Hariharan, B. Huang, A. di Pietro, T. K. Choueiri, *N. Engl. J. Med.* **2019**, *380*, 1103; d) R. J. Motzer, B. Escudier, D. F. McDermott, S. George, H. J. Hammers, S. Srinivas, S. S. Tykodi, J. A. Sosman, G. Procopio, E. R. Plimack, D. Castellano, T. K. Choueiri, H. Gurney, F. Donskov, P. Bono, J. Wagstaff, T. C. Gauler, T. Ueda, Y. Tomita, F. A. Schutz, C. Kollmannsberger, J. Larkin, A. Ravaud, J. S. Simon, L. A. Xu, I. M. Waxman, P. Sharma, I. CheckMate, *N. Engl. J. Med.* **2015**, *373*, 1803; e) R. Motzer, B. Alekseev, S. Y. Rha, C. Porta, M. Eto, T. Powles, V. Grunwald, T. E. Hutson, E. Kopyltsov, M. J. Mendez-Vidal, V. Kozlov, A. Alyasova, S. H. Hong, A. Kapoor, T. A. Gordoa, J. R. Merchan, E. Winquist, P. Maroto, J. C. Goh, M. Kim, H. Gurney, V. Patel, A. Peer, G. Procopio, T. Takagi, B. Melichar, F. Rolland, U. De Giorgi, S. Wong, J. Bedke, et al., *N. Engl. J. Med.* **2021**, *384*, 1289.

[3] a) R. J. Motzer, B. I. Rini, D. F. McDermott, B. G. Redman, T. M. Kuzel, M. R. Harrison, U. N. Vaishampayan, H. A. Drabkin, S. George, T. F. Logan, K. A. Margolin, E. R. Plimack, A. M. Lambert, I. M. Waxman, H. J. Hammers, *J. Clin. Oncol.* **2015**, *33*, 1430; b) D. F. McDermott, J.-L. Lee, C. Szczylik, F. Donskov, J. Malik, B. Y. Alekseev, J. M. G. Larkin, V. B. Matveev, R. A. Gafanov, P. Tomczak, S. S. Tykodi, P. F. Geertsen, P. J. Wiechno, S. J. Shin, F. Pouliot, T. A. Gordoa, W. Li, R. F. Perini, C. Schloss, M. B. Atkins, *J. Clin. Oncol.* **2018**, *36*, 4500; c) R. Nanda, L. Q. Chow, E. C. Dees, R. Berger, S. Gupta, R. Geva, L. Pusztai, K. Pathiraja, G. Aktan, J. D. Cheng, V. Karantza, L. Buisseret, *J. Clin. Oncol.* **2016**, *34*, 2460.

[4] S. Hegde, A. M. Leader, M. Merad, *Immunity* **2021**, *54*, 875.

[5] a) A. Orillion, A. Hashimoto, N. Damayanti, L. Shen, R. Adelaiye-Ogala, S. Arisa, S. Chintala, P. Ordentlich, C. Kao, B. Elzey, D. Gabrilovich, R. Pili, *Clin. Cancer Res.* **2017**, *23*, 5187; b) J. Li, X. Shu, J. Xu, S. M. Su, U. I. Chan, L. Mo, J. Liu, X. Zhang, R. Adhav, Q. Chen, Y. Wang, T. An, X. Zhang, X. Lyu, X. Li, J. H. Lei, K. Miao, H. Sun, F. Xing, A. Zhang, C. Deng, X. Xu, *Nat. Commun.* **2022**, *13*, 1481; c) A. O. Adeshakin, W. Liu, F. O. Adeshakin, L. O. Afolabi, M. Zhang, G. Zhang, L. Wang, Z. Li, L. Lin, Q. Cao, D. Yan, X. Wan, *Cell. Immunol.* **2021**, *362*, 104286.

[6] K. Bi, M. X. He, Z. Bakouny, A. Kanodia, S. Napolitano, J. Wu, G. Grimaldi, D. A. Braun, M. S. Cuoco, A. Mayorga, L. DelloStritto, G. Bouchard, J. Steinharter, A. K. Tewari, N. I. Vokes, E. Shannon, M. Sun, J. Park, S. L. Chang, B. A. McGregor, R. Haq, T. Denize, S. Signoretti, J. L. Guerriero, S. Vigneau, O. Rozenblatt-Rosen, A. Rotem, A. Regev, T. K. Choueiri, E. M. Van Allen, *Cancer Cell* **2021**, *39*, 649.

[7] a) Y. Zhang, S. Choksi, K. Chen, Y. Pobezinskaya, I. Linnoila, Z. G. Liu, *Cell Res.* **2013**, *23*, 898; b) B. Griess, S. Mir, K. Datta, M. Teoh-Fitzgerald, *Free Radical Biol. Med.* **2020**, *147*, 48.

[8] D. Laoui, E. Van Overmeire, G. Di Conza, C. Aldeni, J. Keirsse, Y. Morias, K. Movahedi, I. Houbracken, E. Schouppe, Y. Elkrim, O. Karroum, B. Jordan, P. Carmeliet, C. Gysemans, P. De Baetselier, M. Mazzone, J. A. Van Ginderachter, *Cancer Res.* **2014**, *74*, 24.

[9] a) M. Jiang, X. Li, J. Zhang, Y. Lu, Y. Shi, C. Zhu, Y. Liu, B. Qin, Z. Luo, Y. Du, L. Luo, L. Peng, J. You, *ACS Nano* **2021**, *15*, 14522; b) M. Song, T. Liu, C. Shi, X. Zhang, X. Chen, *ACS Nano* **2016**, *10*, 633.

[10] a) M. L. Guevara, F. Persano, S. Persano, *Semin. Cancer Biol.* **2021**, *69*, 238; b) S. Xu, H. He, Z. Liu, *Chin. J. Chem.* **2022**, *40*, 635.

[11] a) W. P. Su, L. C. Chang, W. H. Song, L. X. Yang, L. C. Wang, Z. C. Chia, Y. C. Chin, Y. S. Shan, C. C. Huang, C. S. Yeh, *ACS Appl. Mater. Interfaces* **2022**, *14*, 24144; b) L. Li, M. Zhen, H. Wang, Z. Sun, W. Jia, Z. Zhao, C. Zhou, S. Liu, C. Wang, C. Bai, *Nano Lett.* **2020**, *20*, 4487; c) M. P. Plebanek, D. Bhaumik, P. J. Bryce, C. S. Thaxton, *Mol. Cancer Ther.* **2018**, *17*, 686.

[12] a) J. Wu, X. Wang, Q. Wang, Z. Lou, S. Li, Y. Zhu, L. Qin, H. Wei, *Chem. Soc. Rev.* **2019**, *48*, 1004; b) H. Wei, L. Gao, K. Fan, J. Liu, J. He, X. Qu, S. Dong, E. Wang, X. Yan, *Nano Today* **2021**, *40*, 101269; c) L. Huang, J. Chen, L. Gan, J. Wang, S. Dong, *Sci. Adv.* **2019**, *5*, eaav5490; d) M. A. Komkova, E. E. Karyakina, A. A. Karyakin, *J. Am. Chem. Soc.* **2018**, *140*, 11302; e) C. N. Loynachan, A. P. Soleimany, J. S. Dudani, Y. Lin, A. Najer, A. Bekdemir, Q. Chen, S. N. Bhatia, M. M. Stevens, *Nat. Nanotechnol.* **2019**, *14*, 883; f) F. Manea, F. B. Houillon, L. Pasquato, P. Scrimin, *Angew. Chem., Int. Ed. Engl.* **2004**, *116*, 6291; g) F. Natalio, R. Andre, A. F. Hartog, B. Stoll, K. P. Jochum, R. Wever, W. Tremel, *Nat. Nanotechnol.* **2012**, *7*, 530; h) M. Soh, D. W. Kang, H. G. Jeong, D. Kim, D. Y. Kim, W. Yang, C. Song, S. Baik, I. Y. Choi, S. K. Ki, H. J. Kwon, T. Kim, C. K. Kim, S. H. Lee, T. Hyeon, *Angew. Chem., Int. Ed. Engl.* **2017**, *56*, 11399; i) G. Y. Tonga, Y. Jeong, B. Duncan, T. Mizuhara, R. Mout, R. Das, S. T. Kim, Y. C. Yeh, B. Yan, S. Hou, V. M. Rotello, *Nat. Chem.* **2015**, *7*, 597; j) W. Zhang, S. Hu, J. J. Yin, W. He, W. Lu, M. Ma, N. Gu, Y. Zhang, *J. Am. Chem. Soc.* **2016**, *138*, 5860; k) Z. Zhang, X. Zhang, B. Liu, J. Liu, *J. Am. Chem. Soc.* **2017**, *139*, 5412; l) M. Wang, M. Chang, C. Li, Q. Chen, Z. Hou, B. Xing, J. Lin, *Adv. Mater.* **2022**, *34*, 2106010; m) M. Wang, M. Chang, P. Zheng, Q. Sun, G. Wang, J. Lin, C. Li, *Adv. Sci.* **2022**, *9*, 2202332.

[13] C. A. Ferreira, D. Ni, Z. T. Rosenkrans, W. Cai, *Nano Res.* **2018**, *11*, 4955.

[14] C. Xu, X. Qu, *NPG Asia Mater.* **2014**, *6*, e90.

[15] a) T. Pirmohamed, J. M. Dowding, S. Singh, B. Wasserman, E. Heckert, A. S. Karakoti, J. E. King, S. Seal, W. T. Self, *Chem. Commun.* **2010**, *46*, 2736; b) C. Korsvik, S. Patil, S. Seal, W. T. Self, *Chem. Commun.* **2007**, *14*, 1056.

[16] H. Zuo, Y. Hou, Y. Yu, Z. Li, H. Liu, C. Liu, J. He, L. Miao, *ACS Appl. Mater. Interfaces* **2020**, *12*, 55723.

[17] W. Guo, M. Zhang, Z. Lou, M. Zhou, P. Wang, H. Wei, *ChemCatChem* **2019**, *11*, 737.

[18] H. Wu, Q. Sun, J. Chen, G.-Y. Wang, D. Wang, X.-F. Zeng, J.-X. Wang, *Chem. Eng. J.* **2021**, *425*, 130640.

[19] P. Chen, I. Chen, *J. Am. Ceram. Soc.* **1996**, *79*, 1793.

[20] S. Fu, R. Yang, L. Zhang, W. Liu, G. Du, Y. Cao, Z. Xu, H. Cui, Y. Kang, P. Xue, *Biomaterials* **2020**, *257*, 120279.

[21] a) F. Cao, Y. Sang, C. Liu, F. Bai, L. Zheng, J. Ren, X. Qu, *ACS Nano* **2022**, *16*, 15495; b) C. Yang, Y. Zhu, D. Li, Y. Liu, C. Guan, X. Man, S. Zhang, L. Zhang, D. Yang, Y. Xu, *Small* **2021**, *17*, 2101837.

[22] J. D. Hayes, A. T. Dinkova-Kostova, K. D. Tew, *Cancer Cell* **2020**, *38*, 167.

[23] a) A. Thyagarajan, R. P. Sahu, *Integr. Cancer Ther.* **2018**, *17*, 210; b) G. Li, D. Liu, E. T. Kimchi, J. T. Kaifi, X. Qi, Y. Manjunath, X. Liu, T. Deering, D. M. Avella, T. Fox, D. C. Rockey, T. D. Schell, M. Kester, K. F. Staveley-O'Carroll, *Gastroenterology* **2018**, *154*, 1024.

[24] a) D. Vasquez-Dunddel, F. Pan, Q. Zeng, M. Gorbounov, E. Albesiano, J. Fu, R. L. Blosser, A. J. Tam, T. Bruno, H. Zhang, D. Pardoll, Y. Kim, *J. Clin. Invest.* **2013**, *123*, 1580; b) Y. Mao, I. Poschke, E. Wennerberg, Y. Pico de Coana, S. Egyhazi Brage, I. Schultz, J. Hansson, G. Masucci, A. Lundqvist, R. Kiessling, *Cancer Res.* **2013**, *73*, 3877; c) J. Schmielau, O. J. Finn, *Cancer Res.* **2001**, *61*, 4756; d) C. A. Corzo, M. J. Cotter, P. Cheng, F. Cheng, S. Kusmartsev, E. Sotomayor, T. Padhya, T. V. McCaffrey, J. C. McCaffrey, D. I. Gabrilovich, *J. Immunol.* **2009**, *182*, 5693.

[25] T. Fukai, M. Ushio-Fukai, *Antioxid. Redox Signaling* **2011**, *15*, 1583.

[26] a) E. Mohamed, R. A. Sierra, J. Trillo-Tinoco, Y. Cao, P. Innamarato, K. K. Payne, A. de Mingo Pulido, J. Mandula, S. Zhang, P. Thevenot, S. Biswas, S. K. Abdalla, T. L. Costich, K. Hanggi, C. M. Anadon, E. R. Flores, E. B. Haura, S. Mehrotra, S. Pilon-Thomas, B. Ruffell, D. H. Munn, J. R. Cubillos-Ruiz, J. R. Conejo-Garcia, P. C. Rodriguez, *Immunity* **2020**, *52*, 668; b) T. Condamine, V. Kumar, I. R. Ramachandran, J. I. Youn, E. Celis, N. Finnberg, W. S. El-Deiry, R. Winograd, R. H. Vonderheide, N. R. English, S. C. Knight, H. Yagita, J. C. McCaffrey, S. Antonia, N. Hockstein, R. Witt, G. Masters, T. Bauer, D. I. Gabrilovich, *J. Clin. Invest.* **2014**, *124*, 2626.

[27] a) L. M. Sanmarco, L. M. Visconti, N. Eberhardt, M. C. Ramello, N. E. Ponce, N. B. Spitale, M. L. Vozza, G. A. Bernardi, S. Gea, A. R. Minguez, M. P. Aoki, *Front. Immunol.* **2016**, *7*, 626; b) S. Nagaraj, A. G. Schrum, H. I. Cho, E. Celis, D. I. Gabrilovich, *J. Immunol.* **2010**, *184*, 3106; c) S. Nagaraj, K. Gupta, V. Pisarev, L. Kinarsky, S. Sherman, L. Kang, D. L. Herber, J. Schneck, D. I. Gabrilovich, *Nat. Med.* **2007**, *13*, 828; d) B. Molon, S. Ugel, F. Del Pozzo, C. Soldani, S. Zilio, D. Avella, A. De Palma, P. Mauri, A. Monegal, M. Rescigno, B. Savino, P. Colombo, N. Jonjic, S. Pecanic, L. Lazzarato, R. Fruttero, A. Gasco, V. Bronte, A. Viola, *J. Exp. Med.* **2011**, *208*, 1949.

[28] a) B. Z. Qian, J. W. Pollard, *Cell* **2010**, *141*, 39; b) J. Lan, L. Sun, F. Xu, L. Liu, F. Hu, D. Song, Z. Hou, W. Wu, X. Luo, J. Wang, X. Yuan, J. Hu, G. Wang, *Cancer Res.* **2019**, *79*, 146.

[29] Q. Xu, S. Choksi, J. Qu, J. Jang, M. Choe, B. Banfi, J. F. Engelhardt, Z. G. Liu, *J. Biol. Chem.* **2016**, *291*, 20030.

[30] S. Zanganeh, G. Hutter, R. Spitler, O. Lenkov, M. Mahmoudi, A. Shaw, J. S. Pajarinen, H. Nejadnik, S. Goodman, M. Moseley, L. M. Coussens, H. E. Daldrup-Link, *Nat. Nanotechnol.* **2016**, *11*, 986.

[31] X. Chen, E. Song, *Nat. Rev. Drug Discovery* **2019**, *18*, 99.

[32] a) M. Yang, J. Li, P. Gu, X. Fan, *Bioact. Mater.* **2021**, *6*, 1973; b) L. Alili, M. Sack, A. S. Karakoti, S. Teuber, K. Puschmann, S. M. Hirst, C. M. Reilly, K. Zanger, W. Stahl, S. Das, S. Seal, P. Brenneisen, *Biomaterials* **2011**, *32*, 2918.

[33] P. J. Siska, K. E. Beckermann, F. M. Mason, G. Andrejeva, A. R. Greenplate, A. B. Sendor, Y. J. Chiang, A. L. Corona, L. F. Gemta, B. G. Vincent, R. C. Wang, B. Kim, J. Hong, C. L. Chen, T. N. Bullock, J. M. Irish, W. K. Rathmell, J. C. Rathmell, *JCI Insight* **2017**, *2*, e93411.

[34] a) L. Y. Dirix, I. Takacs, G. Jerusalem, P. Nikolinakos, H. T. Arkenau, A. Forero-Torres, R. Boccia, M. E. Lippman, R. Somer, M. Smakal, L. A. Emens, B. Hrinczenko, W. Edenfield, J. Gurtler, A. von Heydebreck, H. J. Grote, K. Chin, E. P. Hamilton, *Breast Cancer Res. Treat.* **2018**, *167*, 671; b) S. Adams, P. Schmid, H. S. Rugo, E. P. Winer, D. Loirat, A. Awada, D. W. Cescon, H. Iwata, M. Campone, R. Nanda, R. Hui, G. Curigliano, D. Toppmeyer, J. O'Shaughnessy, S. Loi, S. Paluch-Shimon, A. R. Tan, D. Card, J. Zhao, V. Karantza, J. Cortes, *Ann. Oncol.* **2019**, *30*, 397; c) P. Schmid, C. Cruz, F. S. Braiteh, J. P. Eder, S. Tolaney, I. Kuter, R. Nanda, C. Chung, P. Cassier, J.-P. Delord, M. Gordon, Y. Li, B. Liu, C. O'Hear, M. Fasso, L. Molinero, L. A. Emens, *Cancer Res.* **2017**, *77*, 2986.

[35] a) A. H. Rossevold, N. K. Andresen, C. A. Bjerre, B. Gilje, E. H. Jakobsen, S. X. Raj, R. S. Falk, H. G. Russnes, T. Jahr, R. R. Mathiesen, J. Lomo, O. Garred, S. K. Chauhan, R. R. Lereim, C. Dunn, B. Naume, J. A. Kyte, *Nat. Med.* **2022**, *28*, 2573; b) D. Miles, J. Gligorov, F. Andre, D. Cameron, A. Schneeweiss, C. Barrios, B. Xu, A. Wardley, D. Kaen, L. Andrade, V. Semiglazov, M. Reinisch, S. Patel, M. Patre, L. Morales, S. L. Patel, M. Kaul, T. Barata, J. O'Shaughnessy, I. M. investigators, *Ann. Oncol.* **2021**, *32*, 994.

[36] X. Liu, J. Wu, Q. Liu, A. Lin, S. Li, Y. Zhang, Q. Wang, T. Li, X. An, Z. Zhou, M. Yang, H. Wei, *J. Mater. Chem. B* **2021**, *9*, 7238.

[37] a) X. Zhang, R. Goncalves, D. M. Mosser, *Curr. Protoc. Immunol.* **2008**, *83*, 14; b) W. Diao, F. Jin, B. Wang, C. Y. Zhang, J. Chen, K. Zen, L. Li, *Protein Cell* **2014**, *5*, 714.